Coulomb scattering cross section in a two-dimensional electron gas and production of entangled electrons

D. S. Saraga,[1] B. L. Altshuler,[2] Daniel Loss,[1] and R. M. Westervelt[3]
[1]*Department of Physics and Astronomy, University of Basel, Klingelbergstrasse 82, CH-4056 Basel, Switzerland*
[2]*Physics Department, Princeton University, Princeton, New Jersey 08544, USA*
and NEC Research Institute, 4 Independence Way, Princeton, New Jersey 08540, USA
[3]*Division of Engineering and Applied Sciences, Harvard University, Cambridge, Massachusetts 02138, USA*
(Received 16 August 2004; published 28 January 2005)

We calculate the Coulomb scattering amplitude for two electrons injected with opposite momenta in an interacting two-dimensional electron gas (2DEG). We include the effect of the Fermi-liquid background by solving the two-dimensional (2D) Bethe-Salpeter equation for the two-particle Green function vertex in the ladder and random phase approximations. This result is used to discuss the feasibility of producing spin-EPR pairs in a 2DEG by collecting electrons emerging from collisions at a $\pi/2$ scattering angle, where only the entangled spin singlets avoid the destructive interference resulting from quantum indistinguishability. Furthermore, we study the effective 2D electron-electron interaction due to the exchange of virtual acoustic and optical phonons and compare it to the Coulomb interaction. Finally, we show that the 2D Kohn-Luttinger pairing instability for the scattering electrons is negligible in a GaAs 2DEG.

DOI: 10.1103/PhysRevB.71.045338 PACS number(s): 73.23.−b, 03.67.Mn, 71.10.Ca

I. INTRODUCTION

Recent experiments[1,2] have allowed for the imaging of the coherent electron flow in a two-dimensional electron gas (2DEG), demonstrating a roughly directional injection through a quantum-point contact (QPC) tuned to its lowest transversal mode. We propose here to use such a setup to investigate Coulomb scattering in 2D, by measuring the scattering cross section. This provides a natural motivation for solving a long-lasting problem in Fermi-liquid theory: finding the scattering amplitude for the Coulomb interaction in a 2D system, including the effect of the many-particle background of the interacting Fermi sea. We derive[3] the scattering amplitude f by solving the Bethe-Salpeter equation in the ladder approximation and for electrons in the Cooper channel (opposite momenta).[4,5] This solution provides a useful addition to Fermi-liquid theory applied to electron-electron interaction. The development of Fermi-liquid theory, which goes back over many decades, includes discussions of screening,[6] the lifetime of quasiparticles,[7,8] the renormalization factor Z of the Green function,[9,10] the effective mass,[10,11] and scattering.[12–14] An additional issue is how strongly the Coulomb scattering is affected by the effective electron-electron interaction mediated by the exchange of virtual phonons, which have been studied, for instance, in the context of Coulomb drag (see, e.g., Ref. 15) and screening.[16] Another extension concerns the effect of lower dimensionality[13,17] in Kohn-Luttinger superconductivity,[12] and the question of the strength of superconducting fluctuations (if any), which could, in principle, spoil the Coulomb scattering.

A second motivation for this work comes from the current efforts devoted to solid-state implementations of quantum information protocols using the spin of individual electrons as qubits.[18–20] In particular, the experimental demonstration of entangled (EPR) pairs of spin-qubit is still a present-day challenge and has motivated a number of theoretical proposals for *entanglers*, i.e., devices creating mobile (spin-) entangled electrons. These proposals relied on energy filtering via quantum dots[18,21–23] and carbon nanotubes,[24] and/or the use of superconductors.[21,24–26] Other schemes are in closer relation with optics, and use beam splitters for spin,[27] orbital,[28] or particle-hole entanglement.[29,30]

We propose[3] here a simple idea for the creation of spin-entangled pairs in a 2DEG, inspired by the well-known interference effect found *in vacuum* for the scattering of indistinguishable particles.[31,32] Using the fact that electron pairs in the singlet (triplet) spin state behave like spinless bosons (fermions) in spin-independent collisions, we propose to collect electrons emerging from electron-electron collisions with a scattering angle $\theta=\pi/2$. In this situation, the destructive interference is complete for triplets; hence, the collected electrons must be in the entangled singlet state $|S\rangle=(|\uparrow\downarrow\rangle-|\downarrow\uparrow\rangle)/\sqrt{2}$, which is one the EPR states desirable for quantum information protocols. The question now arises whether this two-particle exchange effect survives in the presence of a sea of interacting electrons. Using our solution for the scattering amplitude f, we will show that the entanglement created (or rather, postselected) by the collision should be observable in a realistic 2DEG.

We emphasize that our study of electron-electron interaction is motivated by the prospect of seeing experimental control on the propagation of electrons in 2DEGs and on their quasiparticle properties. The experiments of Refs. 1 and 2 have used electron scattering off a scanning probe microscope (SPM) tip to image both quantum interferences and raylike propagation of electrons, including diffraction. They have also shown control over the quasiparticle lifetimes for hot electrons, in good agreement with Fermi-liquid theory. The theoretical work presented here indicate that such experimental studies can be extended to more general Fermi-liquid effects involving two quasiparticles.[33]

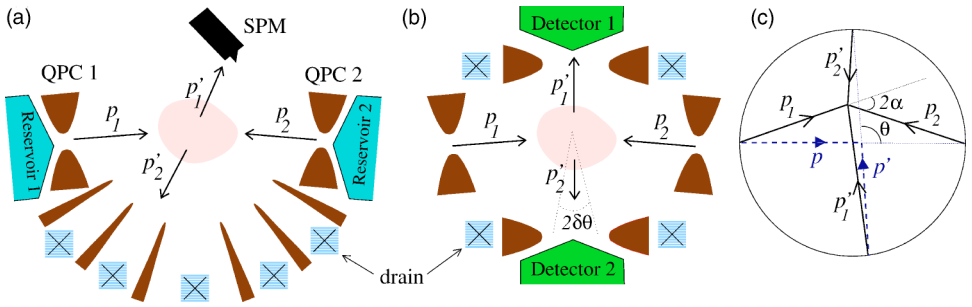

FIG. 1. *Setup*. Two quantum-point contacts allow the injection of electrons from two reservoirs with initial momenta $\mathbf{p}_1 \simeq -\mathbf{p}_2$. (a) Measuring the conductance as a function of the SPM tip position gives an estimate of the electron flux[1] and, thereby, of the differential scattering length $\lambda(\theta)$ (top). Alternatively, one can define "bins" spanning different angles and collect the current in the drain contacts (bottom). (b) *EPR setup*. The electrons are collected in two detectors (with an aperture angle $2\delta\theta$) placed such that only electrons emerging from collisions with a scattering angle around $\pi/2$ are detected. Because of antisymmetrization, the scattering amplitude identically vanishes for the spin-triplet states, allowing only the spin-entangled singlets (EPR pairs) to be collected. (c) *Scattering parameters*. The initial $(\mathbf{p}_1,\mathbf{p}_2)$ and final $(\mathbf{p}_1',\mathbf{p}_2')$ momenta are connected by a circle of radius $p'=p$ due to energy and momentum conservation, where the relative momenta are $\mathbf{p}=(\mathbf{p}_1-\mathbf{p}_2)/2$, $\mathbf{p}'=(\mathbf{p}_1'-\mathbf{p}_2')/2$ and $\theta=\angle(\mathbf{p},\mathbf{p}')$ is the scattering angle. The Cooper channel is defined by $2\alpha=\angle(\mathbf{p}_1,-\mathbf{p}_2)\to 0$.

We start in Sec. II by describing the envisioned setup and the mechanism for the production of EPR pairs. We write down in Sec. III the problem in a Fermi-liquid approach and solve the Bethe-Salpeter equation in the ladder approximation, using random-phase approximation (RPA) and considering the Cooper channel (opposite incident momenta). The solution for the scattering amplitude (the t matrix) is written in Eq. (38) in terms of a Fourier series, with explicit expressions for the coefficients. We study in Sec. IV the scattering cross section and address in more detail the issue of the production and detection of the EPR pairs. We investigate in Sec. V the electron-electron interaction mediated by phonons and show that it does not have a significant effect on scattering. In Sec. VI we show that no superconducting instabilities arise from the Kohn-Luttinger mechanism.[12] We finally consider in more detail the case of small r_s in the Appendixes. We derive in Appendix A analytical expressions for the scattering amplitude and its derivative at $\theta=\pi/2$. In Appendix B we develop a different calculation valid for very small r_s, which is needed to estimate the contribution of forward-scattering states.

II. SETUP AND PRODUCTION OF EPR PAIRS

The setup for the study of Coulomb collisions in a 2DEG is described in Fig. 1. Two quantum point contacts (QPC) tuned into their lowest transversal mode filter electrons escaping from two thermal reservoirs,[1] and allow them to collide with incident momenta $\mathbf{p}_1 \simeq -\mathbf{p}_2$ and final momenta $\mathbf{p}_1',\mathbf{p}_2'$. A way to measure the scattering length is to use a SPM tip and to record the conductance across the sample, which provides an estimate for the local electron flux;[1] alternatively, one can define "bins" spanning different angles and collect the current in the drain contacts [see Fig. 1(a)]. For the production of EPR pairs, described in Fig. 1(b), the electrons are collected at two detectors placed so that only collisions with a scattering angle θ within a small window $\delta\theta$ around $\pi/2$ are collected: $\theta \in [\pi/2-\delta\theta, \pi/2+\delta\theta]$. We introduce the conserved total momentum $\mathbf{P}=\mathbf{p}_1+\mathbf{p}_2=\mathbf{p}_1'+\mathbf{p}_2'$, the relative momenta $\mathbf{p}=\frac{1}{2}(\mathbf{p}_1-\mathbf{p}_2)$, $\mathbf{p}'=\frac{1}{2}(\mathbf{p}_1'-\mathbf{p}_2')$, and the scattering angle $\theta=\angle(\mathbf{p}',\mathbf{p})$ [see Fig. 1(c)]. The most favorable arrangement is the Cooper channel[5]

$$\mathbf{p}_2 \simeq -\mathbf{p}_1, \tag{1}$$

as it yields conservation of the individual energies: $p_1 \simeq p_2 \simeq p_1' \simeq p_2'$, where $p_i=|\mathbf{p}_i|$. As a consequence, the scattering angle $\theta \simeq \angle(\mathbf{p}_1',\mathbf{p}_1)$ can be easily determined, while the EPR pairs have the same energy and should therefore arrive in the detectors at the same time. We consider incoming electrons with small excitation energies $\xi_i=\hbar^2 p_i^2/2m-E_F \ll E_F$ above the Fermi energy $E_F=\hbar^2 k_F^2/2m$ of the 2DEG (m is the effective mass).[34]

Now we describe in more detail the production of spin-entangled electrons. First, we use the fact that the two-particle interference is totally destructive for fermions colliding with a scattering angle $\theta=\pi/2$, while, in contrast, the scattering of bosons is enhanced compared to the classical value. This is seen in the corresponding cross sections $\sigma_{B/F}=|f(\theta)\pm f(\pi-\theta)|^2$. Second, the fermionic character of a pair of particles also depends on its spin state:[9,31,32] a spin-singlet electron pair

$$|S\rangle = (|\uparrow\downarrow\rangle - |\downarrow\uparrow\rangle)/\sqrt{2} \tag{2}$$

behaves, in a spin-independent collision, like a bosonic pair because of its symmetrical orbital wave function, while the triplets

$$|T_0\rangle = (|\uparrow\downarrow\rangle + |\downarrow\uparrow\rangle)/\sqrt{2}; \quad |T_\pm\rangle = |\uparrow\uparrow\rangle, |\downarrow\downarrow\rangle \tag{3}$$

behave like fermions. It is then clear that a $\pi/2$ scattering experiment could distill the singlet part of uncorrelated pairs of electrons—at least in free space.

It might seem surprising to be able to collect spin-singlet states when starting from two electrons having no spin correlations (they come from two independent unpolarized reservoirs). However, a spin-singlet component is always present, as seen from the change of basis for the density matrix describing the two-spin state

$$\rho = \frac{1}{4}\mathbb{1} = \frac{1}{4}\sum_{\sigma,\sigma'=\uparrow,\downarrow} |\sigma\sigma'\rangle\langle\sigma\sigma'| = \frac{1}{4}|S\rangle\langle S| + \frac{1}{4}\sum_{\mu=0,\pm} |T_\mu\rangle\langle T_\mu|, \tag{4}$$

where $|\sigma\sigma'\rangle$ corresponds to the two-electron state where the electron injected from the first (second) reservoir has spin σ (σ').

A real detector has a small, but finite aperture angle $2\delta\theta$ around $\theta=\pi/2$, so that triplets will always be present. To examine the efficiency of this collision entangler, we will define the ratio $\mathcal{R}$ between the number of scattered triplets and singlets $N_{T/S}$ in Sec. IV. We will find

$$\mathcal{R} = \frac{N_T}{N_S} \simeq \delta\theta^2 \left|\frac{f'(\pi/2)}{f(\pi/2)}\right|^2 \tag{5}$$

and show that $|f'/f|^2 \sim 1$ at $\theta=\pi/2$. Therefore, the number of triplets, which we want to avoid as they can be in an unentangled product state $|T_\pm\rangle$, is negligible for small $\delta\theta$.

III. CALCULATION OF THE SCATTERING AMPLITUDE

In this section we study the scattering between two electrons that are both above the Fermi surface—as opposed to the standard calculation of the electron lifetime due to scattering of one electron above the surface with all the electrons present below the surface.[5,6] We consider a clean 2D Fermi liquid with Coulomb interaction, neglecting impurity scattering (the mean-free path can be around 10 μm, which is larger than the size $L\simeq 1$ μm of the envisioned setup[1]). The effect of phonons will be considered in Sec. V.

A. RPA and Bethe-Salpeter equation

In 2D, the scattering amplitude f for two particles with a relative momentum $\mathbf{p}$ is linked to the t matrix via the relation[35]

$$f(\theta) = -\frac{m}{\hbar^2\sqrt{2\pi p}} t(\theta), \tag{6}$$

with the corresponding scattering cross section ("length" in 2D) $\lambda(\theta)=|f(\theta)|^2$. The 2D Coulomb interaction in vacuum is[36,37]

$$V_C(\mathbf{q}) = \int d\mathbf{r} e^{-i\mathbf{q}\cdot\mathbf{r}} V_C(r) = \frac{2\pi e_0^2}{q}, \tag{7}$$

where $e_0^2=e^2/4\pi\epsilon_0\epsilon_r$. We included the dielectric constant ϵ_r of GaAs and set $p=k_F$ for future comparisons with the scattering in GaAs. The corresponding exact scattering t matrix is given by[35]

$$t_C(\theta) = \frac{\varsigma}{\sin|\theta/2|}\frac{\hbar^2\sqrt{\pi}}{m}\frac{\Gamma\left(\frac{1}{2}+i\varsigma\right)}{\Gamma(1-i\varsigma)} e^{i\pi/4-2i\varsigma\ln|\sin\theta/2|}, \tag{8}$$

with $\Gamma(x)$ the gamma function and $\varsigma=me_0^2/k_F\hbar^2$. This yields

$$|t_C(\theta)| = \frac{\hbar^2\sqrt{\pi\varsigma\tanh(\pi\varsigma)}}{m\sin|\theta/2|}. \tag{9}$$

Note that $|t_C| \neq V_C$, contrary to the situation in 3D.

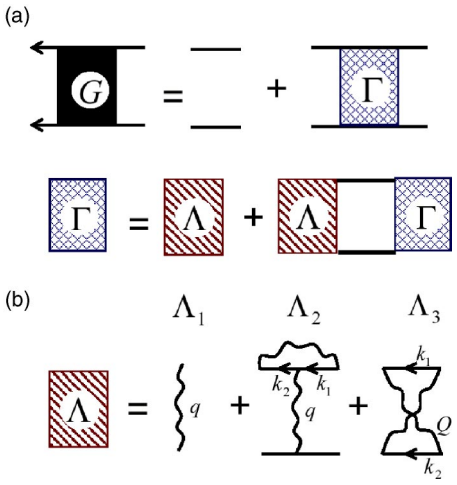

FIG. 2. (a) The two-particle Green function and the Bethe-Salpeter equation for the vertex Γ. We only show the direct diagrams (i.e., without the exchange ones). (b) Lowest-order diagrams ($\Lambda_{1,2,3}$) contributing to the irreducible vertex Λ. The wavy lines denote the screened Coulomb interaction V, given in RPA by resuming the bubble diagrams.

Next we include the effect of the many-particle background and calculate the t matrix in the presence of the Fermi sea. The t matrix is given by the vertex function $t=\Gamma(\omega_{1,2}\to\xi_{1,2})$ appearing in the two-particle Green function[4] [see Fig. 2(a)]. We note that the arrangement $\mathbf{p}_2=-\mathbf{p}_1$ corresponds to the well-known Cooper channel, discussed, for instance, in the context of Cooper instability.[5] Consequently, we adopt the approach used by Kohn and Luttinger in their work on intrinsic superconductivity in a 3D Fermi liquid.[12] However, our calculation differs in two ways. First, we consider a 2D system where the screened potential is nonanalytic (because of the modulus $q=|\mathbf{q}|$ instead of q^2 in 3D). Second, we are interested in the scattering amplitude, while Kohn and Luttinger focused on the instability in the vertex arising from spherical harmonics of the crossed ("exchange") diagram (see Λ_3 below).

The two-particle Green function in real space is

$$G_{\sigma_1'\sigma_2'\sigma_1\sigma_2}(1',2';1,2) = (-i)^2\langle \mathcal{T} c_{1'\sigma_1'} c_{2'\sigma_2'} c_{1\sigma_1}^\dagger c_{2\sigma_2}^\dagger\rangle, \tag{10}$$

with the notation $i=(\mathbf{x}_i,t_i)$, $\sigma_i=\uparrow,\downarrow$ are the spin indices, and $\mathcal{T}$ the time-ordering operator. For a spin-independent Hamiltonian we can write[4,12]

$$\begin{aligned} G_{\sigma_1'\sigma_2'\sigma_1\sigma_2}&(1',2';1,2) \\ &= G(1)G(2)(2\pi)^3 \\ &\quad\times[\delta(1'-1)\delta_{\sigma_1'\sigma_1}\delta_{\sigma_2'\sigma_2} - \delta(1'-2)\delta_{\sigma_1'\sigma_2}\delta_{\sigma_2'\sigma_1}] \\ &\quad + (i/\hbar)G(1')G(2')\Gamma_-(1',2';1,2)G(1)G(2), \end{aligned} \tag{11}$$

with the single-particle Green function $G(i)$ and the (anti-)symmetrized vertex $\Gamma_\pm(1',2';1,2)=\Gamma(1',2';1,2)\pm\Gamma(1',2';2,1)$, expressed in terms of the unsymmetrized Γ. We consider the singlet and triplet basis $\{|S\rangle,|T_0\rangle,|T_\pm\rangle\}$ and

introduce the corresponding creation operators

$$a^{\dagger}_{S/T_0}(1,2) = 1/\sqrt{2}(c^{\dagger}_{1\uparrow}c^{\dagger}_{2\downarrow} \mp c^{\dagger}_{1\downarrow}c^{\dagger}_{2\uparrow}), \tag{12}$$

$$a^{\dagger}_{T_{\pm}}(1,2) = c^{\dagger}_{1\uparrow}c^{\dagger}_{2\uparrow}, c^{\dagger}_{1\downarrow}c^{\dagger}_{2\downarrow}, \tag{13}$$

which we use to define the related two-particle Green functions

$$G_{S/T_0}(1',2';1,2) = -\langle \mathcal{T} a_{S/T_0}(1',2') a^{\dagger}_{S/T_0}(1,2)\rangle = \tfrac{1}{2}\{G_{\uparrow\downarrow\uparrow\downarrow} + G_{\downarrow\uparrow\downarrow\uparrow} \mp G_{\uparrow\downarrow\downarrow\uparrow} \mp G_{\downarrow\uparrow\uparrow\downarrow}\}, \tag{14}$$

$$G_{T_{\pm}}(1',2';1,2) = -\langle \mathcal{T} a_{T_{\pm}}(1',2') a^{\dagger}_{T_{\pm}}(1,2)\rangle = G_{\uparrow\uparrow\uparrow\uparrow,\downarrow\downarrow\downarrow\downarrow}, \tag{15}$$

where we have dropped the argument $(1',2';1,2)$ for ease of notation. Using (11), we find that the spin and orbital symmetry of the pair of particles is directly reflected in the vertex Γ

$$G_{S/T}(1',2';1,2) = -G(1)G(2)[\delta(1'-1) \pm \delta(1'-2)](2\pi)^3 + (i/\hbar)G(1')G(2')\Gamma_{\pm}(1',2';1,2)G(1)G(2), \tag{16}$$

where T denotes one of the triplet states $T_{0,\pm}$. From Eq. (16) we see that the vertex (and, therefore, the scattering amplitude) has either a bosonic (symmetric) or fermionic (antisymmetric) behavior, depending on the spin state. Therefore, we calculate the *unsymmetrized* vertex Γ giving the t-matrix t and the scattering amplitude f, and (anti)symmetrize the latter according to the spin state.

From now on we consider the Green function in momentum and frequency space. Taking into account conservation of momentum and frequency, the vertex satisfies the Bethe-Salpeter equation[4,12]

$$\Gamma(\tilde{p}',\tilde{p};\tilde{P}) = \Lambda(\tilde{p}',\tilde{p};\tilde{P}) + \frac{i}{\hbar(2\pi)^3}\int d\tilde{k}\Lambda(\tilde{k},\tilde{p};\tilde{P}) \times G(\tilde{k}_1)G(\tilde{k}_2)\Gamma(\tilde{p}',\tilde{k};\tilde{P}), \tag{17}$$

illustrated in Fig. 2(a). We have introduced the irreducible vertex Λ, the intermediate momenta $\tilde{k}_{1,2} = \tilde{P}/2 \pm \tilde{k}$ given in terms of the relative momentum $\tilde{k}$, the frequency ω, and the notation $\tilde{p} = (\mathbf{p}, \omega)$. All the possible exchange diagrams should be included in Λ while avoiding double-counting physically equivalent diagrams. We first consider zero temperature $k_B T = 0$, and discuss finite T effects later.

In a first stage, we use the random-phase approximation (RPA) for the many-electron background.[4] This yields the screened interaction

$$V(\tilde{q}) = \frac{V_C(q)}{1 - V_C(q)\chi^0(\tilde{q})}, \tag{18}$$

given in terms of the bubble susceptibility χ^0, with the momentum transfer $\tilde{q} = (\mathbf{q}, \omega_q) = \tilde{p}' - \tilde{p}$. The RPA requires a high density, which is controlled in 2D via the parameter $r_s = me_0^2/(\hbar^2\sqrt{\pi n}) \ll 1$, where n is the electronic sheet density. First, one can consider the static limit[6]

$$\chi^0(q, \omega_q = 0) = -\frac{m}{\pi\hbar^2}\left[1 - \Theta(q > 2k_F)\sqrt{1 - \left(\frac{2k_F}{q}\right)^2}\right] \tag{19}$$

because the dependence of χ^0 with ω_q is smooth and, therefore, can be neglected in the integration of intermediate fermionic lines, which, as we shall see below, selects only intermediate states $\mathbf{k}$ at the Fermi surface: $\xi_k = 0 \Rightarrow \hbar\omega_q = \xi_k - \xi_1 = 0$ for $\xi_1 = 0$. Note that the divergence in the ω_q integration of $V(\tilde{q}) \sim 1/(\omega_q - \omega_p)$ near the plasmon frequency ω_p disappears because it is an odd function of ω. Next, the q-dependent part of $\chi^0(q, \omega_q = 0)$ in 2D vanishes at the Fermi surface, as $q \simeq 2k_F \sin|\theta/2| < 2k_F$. This justifies the standard Thomas-Fermi screening

$$V(q) = \frac{2\pi e_0^2}{q + k_s}, \tag{20}$$

with the screening momentum $k_s = 2me_0^2/\hbar^2 = k_F r_s\sqrt{2}$.

Within RPA, the renormalized one-particle Green function is given by[5]

$$G(\tilde{k}) \simeq \frac{Z}{\omega_k - \xi_k^* - i\,\mathrm{Im}\,\Sigma(\tilde{k})} \tag{21}$$

for small ω_k and ξ_k. In 2D, for GaAs and $k_B T, \xi_k \to 0$, one has the renormalization factor[9,10] $Z = 1 - r_s(1/2 - 1/\pi)/\sqrt{2} \simeq 0.62$, the renormalized mass[10] $m^* = m[1 - \ln(1/r_s)r_s/\pi] \simeq 0.96m$ entering in ξ_k^*, and the broadening (inverse lifetime)[7] $\mathrm{Im}\Sigma \sim \xi^2 \ln\xi$. The latter vanishes for particles near the Fermi surface ($\xi_k \to 0$), which corresponds to well-defined quasiparticle states. For simplicity,[38] we set $Z = 1$, $m^* = m$, and, therefore, approximate the renormalized Green function by the free propagator

$$G(\tilde{k}) \simeq G_0(\tilde{k}) = \frac{1}{\omega_k - \xi_k}. \tag{22}$$

We now consider the irreducible vertex Λ in lowest orders in V, as $mV/\pi\hbar^2 \sim me_0^2/k_F \sim r_s \ll 1$. The lowest-order diagrams are shown in Fig. 2(b); they are the single-interaction line Λ_1, the vertex renormalization Λ_2, and the crossed diagram Λ_3

$$\Lambda_1 = V(q), \tag{23}$$

$$\Lambda_2 = V(q)\frac{1}{(2\pi)^2}\int d\mathbf{k}_1 B(\mathbf{k}_1, \tilde{q})[V(\mathbf{k}_1 - \mathbf{p}_1) + V(\mathbf{p}_2' - \mathbf{k}_1)], \tag{24}$$

$$\Lambda_3 = \frac{1}{(2\pi)^2}\int d\mathbf{k}_1 B(\mathbf{k}_1, \tilde{Q})V(\mathbf{k}_1 + \mathbf{p}_2')V(\mathbf{k}_1 + \mathbf{p}_2), \tag{25}$$

with $\tilde{q} = \tilde{p}_1' - \tilde{p}_1$ and $\tilde{Q} = \tilde{p}_2' - \tilde{p}_1$. The function

$$B(\mathbf{k},\tilde{q}) = \frac{n(\mathbf{k}+\mathbf{q}) - n(\mathbf{k})}{\xi_{\mathbf{k}+\mathbf{q}} - \xi_{\mathbf{k}} - \hbar\omega \pm i\eta} \tag{26}$$

arises from the frequency integration of the bubble diagram and involves the Fermi occupation factors $n(\mathbf{k})=\Theta(-\xi_k)$ at $k_BT=0$. We can estimate $\Lambda_2 \simeq V(q)V(k_F)\int d\mathbf{k}_1 B(\mathbf{k}_1, \tilde{q})/(2\pi)^2 = V(q)V(k_F)\chi^0(\tilde{q}) \simeq -V(q)k_s/k_F$ (apart from negligibly small integration regions), and similarly for Λ_3. Hence,[39] $\Lambda_{2,3}/\Lambda_1 \sim r_s \ll 1$ and we can keep only the single-interaction line $\Lambda \simeq \Lambda_1 = V$, which corresponds to the *ladder approximation*. The criterion for the validity of the ladder approximation is usually expressed[4] by $\lambda k_F \ll 1$. This low-density regime is nevertheless consistent with RPA, as can be seen, e.g., from the Born approximation

$$t \simeq V_C \Rightarrow \lambda k_F \sim \frac{1}{2\pi}\left[\frac{mV_C(k_F)}{\hbar^2}\right]^2 \sim \left(\frac{k_s}{k_F}\right)^2 \ll 1. \tag{27}$$

In summary, we need to solve the following Bethe-Salpeter equation

$$\Gamma(\tilde{p}' - \tilde{p}; \tilde{P}) = V(p' - p) + \frac{i}{\hbar(2\pi)^3}\int d\tilde{k} V(\tilde{k} - \tilde{p}) \times G_0(\tilde{k}_1)G_0(\tilde{k}_2)\Gamma(\tilde{p}' - \tilde{k}; \tilde{P}), \tag{28}$$

where $\tilde{k}_{1,2} = \frac{1}{2}\tilde{P} \pm \tilde{k}$.

B. Energy integration and logarithmic factor

We now follow the derivation of the Cooper instability,[5] including a discussion of the less standard case of particles that are not in the Cooper channel, i.e., with $\mathbf{p}_1 \neq -\mathbf{p}_2$. Before solving Eq. (28) to all orders, we first consider its second-order iteration, $\Gamma^{(2)}(\mathbf{p}'-\mathbf{p};\tilde{P}) = V(\mathbf{p}'-\mathbf{p}) + i/\hbar(2\pi)^3 \int d\tilde{k} V(\mathbf{k}-\mathbf{p}) G(\tilde{k}_1)G(\tilde{k}_2)V(\mathbf{p}'-\mathbf{k})$. The ω_k integration of the Green functions yields[4]

$$D(\mathbf{k}_1,\mathbf{k}_2) \coloneqq \frac{i}{2\pi\hbar}\int d\omega_k G_0\left(\mathbf{k}_1, \frac{\Omega}{2}+\omega_k\right) G_0\left(\mathbf{k}_2, \frac{\Omega}{2}-\omega_k\right) = \frac{N(k_1,k_2)}{\xi_1 + \xi_2 - \xi_{k_1} - \xi_{k_2} + 2i\eta N(k_1,k_2)}, \tag{29}$$

with the function $N(k_1,k_2) \coloneqq 1 - n(k_1) - n(k_2)$. The $\tilde{P}$ frequency $\hbar\Omega$ has been set to $\xi_1+\xi_2$ to retrieve the t matrix, and η can be set to 0 in the denominator. We now consider the Cooper channel $\mathbf{p}=\mathbf{p}_1=-\mathbf{p}_2, \mathbf{k}=\mathbf{k}_1=-\mathbf{k}_2$, which gives $q = |\mathbf{p}'-\mathbf{p}| = 2p\sin|\theta/2|$, and $n(k_1)=n(k_2)=\Theta(-\xi_k) \Rightarrow N(k) = \mathrm{sgn}(\xi_k)$. This yields a single discontinuity in the numerator when $\xi_k=0$, which coincides with the zero of the denominator ($\xi_k=\xi$) when considering a vanishing excitation energy for the incident particles, $\xi=\xi_{1,2}\to 0$.

As a consequence, the main contribution to the energy integration comes from virtual states at the Fermi surface, i.e., $\xi_k \simeq 0$. We set $k=k_F$ in V and integrate only on $D(k) = D(\mathbf{k},\mathbf{k})$. The dominant term comes from both sides around $k=k_F$ and yields the factor[40]

$$\nu \coloneqq \frac{1}{2\pi}\int_0^\infty dk k D(k) \simeq \frac{m}{2\pi\hbar^2}\log\frac{\xi}{E_F}. \tag{30}$$

This logarithmic divergence (as $\xi\to 0$) plays a crucial role here. It allows us to neglect the k dependence of V, as it selects only intermediate states at the Fermi surface (their contribution is logarithmically dominant as $\xi\to 0$). This is the main effect of the fermionic background on the scattering, apart from the screening.

We now consider finite temperatures with $n(k) = (1+e^{\xi_k/k_BT})^{-1}$. For $\xi \sim k_BT \ll E_F$, we find

$$\nu(T) \simeq \frac{m}{4\pi\hbar^2}\left\{\log\frac{\xi^2 - (k_BT)^2}{E_F^2} + \frac{\xi}{k_BT}\left[\log\frac{k_BT-\xi}{k_BT+\xi} - \pi i\right] + 2\right\}. \tag{31}$$

For $\xi \gg k_BT$ we recover (30), while for $\xi \ll k_BT$ we find

$$\nu(T) \simeq \frac{m}{2\pi\hbar^2}\log\frac{k_BT}{E_F}. \tag{32}$$

This logarithmic factor (32) is the 2D equivalent of the one found in the discussion of the Cooper instability for both phonon-mediated[4] or Kohn-Luttinger[12] superconductivity, with the 2D density of state $\nu_{2D} = m/(2\pi\hbar^2)$ instead of the 3D one.

Different cutoffs arise if the Cooper channel condition ($P=0$) is not strictly respected. For instance, experiments might require a small but finite angle $2\alpha = \angle(\mathbf{p}_1, -\mathbf{p}_2) \ll 1$ between the incident particles to prevent misalignment, in which case we have a total momentum $P = 2p_1\sin\alpha \simeq 2k_F\alpha$ if $p_1=p_2$ and $|p_1-k_F|$, $P \ll k_F$. Alternatively, particles might be injected in perfect opposite direction ($\alpha=0$), but with a different energy (this can arise, e.g., in case of hot electrons, see Sec. IV I), i.e., $p_1 \neq p_2$, leading to $P=|p_1-p_2|$. In these cases, we find at $T=0$

$$N(k,\phi) = \Theta(k-k_+) - \Theta(k_- - k), \tag{33}$$

where $k_\pm = \sqrt{k_F^2 - (P\sin\phi)^2} \pm P\cos\phi$, and ϕ is the integration angle for $\mathbf{k}$ [$\phi = \angle(\mathbf{k},\mathbf{p}) + \pi/2$ if $\alpha \neq 0$; $\phi = \angle(\mathbf{k},\mathbf{p})$ if $p_1 \neq p_2$]. In the limit $|p_{1,2}-k_F| \ll P$, we find

$$\nu(\phi) \simeq \frac{m}{2\pi\hbar^2}\log\left(\frac{P}{k_F}\sin|\phi|\right), \tag{34}$$

where we recall that $P = 2k_F\alpha$ or $|p_1-p_2|$.

Therefore, the divergence (due to the single discontinuity of the two Fermi surfaces for particles in the Cooper channel) is cut off by $\max\{\xi/E_F, k_BT/E_F, P/k_F\}$. Away from the Cooper channel ($P \simeq k_F$), or for large temperatures ($k_BT, \xi \simeq E_F$), the logarithmic factor disappears; in that case, the fact that only virtual states having the Fermi energy ($k \simeq k_F$) contribute to higher orders does not apply. When $p_{1,2} \simeq k_F$, we must make sure that the ingoing and outgoing states are available, i.e., $p_{1,2}, p'_{1,2} > k_F$. For $\pi/2$ scattering and $\alpha \neq 0$, we have $p'_{1,2} = p_1(\cos\alpha \pm \sin\alpha) \Rightarrow p_1 \lesssim k_F(1+\alpha)$ [see Fig.

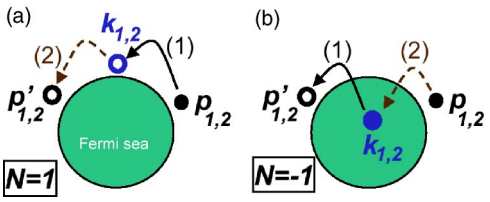

FIG. 3. Scattering with a fermionic background. (a) Direct virtual transition: the initial states $p_{1,2}$ first go to the available intermediate state $k_{1,2}>k_F$ (1), and then go to the final states $p'_{1,2}$ (2). This process is represented by a term $c^\dagger_{p'}c_k c^\dagger_k c_p$. (b) Exchange process corresponding to $c^\dagger_{p'}c^\dagger_k c_k c_p$: intermediate states with $k_{1,2}<k_F$ first fill the final states $p'_{1,2}$, creating a particle-hole excitation (1); the holes are subsequently filled by the initial states $p_{1,2}$ (2). The effect of the many-particle fermionic background manifests itself in the function $N(k_1,k_2)$ in Eq. (29), which adds a negative sign for the exchange process, and is therefore responsible, in the Cooper channel, for the logarithmic term (30) that selects states at the Fermi surface, $k_{1,2}\simeq k_F$. In vacuum, we have only case (a), so $N(k_1,k_2)=1$ and all states contribute with the same sign; this yields no divergence, and therefore no selection.

1(c)], then $\alpha=P/2k_F<\xi/E_F$. Similarly for $p_1\neq p_2$, we need $p_2=p_1-P>k_F\Rightarrow P/2k_F<\xi_1/E_F$. As a consequence, the cutoff is determined by either ξ or k_BT.

Before proceeding with the solution of the Bethe-Salpeter equation, we comment on the difference with the standard scattering theory in vacuum, where the scattering t matrix is given by the Lippmann-Schwinger equation[31] $t^{\rm vac}_E=V+VG^{\rm vac}_E t^{\rm vac}_E$ for an incoming energy E. As the single-particle Green function $G^{\rm vac}_E(\mathbf{k})=1/(E-E_k)$ is an odd function around the divergence at $E_k=E$, no divergence develops and no selection of intermediate states $\mathbf{k}$ occurs.

In the case of a Fermi sea, the Lippmann-Schwinger equation is replaced by the Bethe-Salpeter equation (which can be written symbolically $\Gamma=V+VD\Gamma$), and $G^{\rm vac}_E$ corresponds to the factor D [Eq. (29)]. This is seen by setting $E_F=0$, giving $N(k_1,k_2)\to 1$ and, thus, $D\to G^{\rm vac}_E(k)$ for the relative momentum $\mathbf{k}=(\mathbf{k}_1-\mathbf{k}_2)/2$. The difference between the Fermi sea and the vacuum cases lies in the numerator $N(k_1,k_2)$, which is a direct effect of Fermi statistics and assigns a negative sign to the exchange processes, where the transitions occur via two states $k_1,k_2<k_F$ below the Fermi surface, as compared to the direct processes via intermediate states above the Fermi surface $k_{1,2}>k_F$ (see Fig. 3). In the Cooper channel, this factor is responsible for the selection of intermediate states at the Fermi energy ($k_{1,2}\simeq k_F$) via the logarithmic-divergence (30); the latter arises because $N(k)=\mathrm{sgn}(\xi_k)$ implies that $D(\xi_k)\sim 1/|\xi_k|$ is an even function (after setting $\xi=0$). We emphasize that the selection of virtual states at the Fermi energy ($k\simeq k_F$) disappears away from the Cooper channel [see Eq. (34)].

C. Solution as a Fourier series

We can repeat the integration over the frequency and energy described above at every order. This results in a new Bethe-Salpeter equation

$$t(\theta)=V(\theta)+\nu\frac{1}{2\pi}\int d\phi V(\phi)t(\theta-\phi), \tag{35}$$

with the screened 2D Coulomb potential at the Fermi surface

$$v(\phi)=\frac{2\pi e^2}{2k_F\sin|\phi/2|+k_s}. \tag{36}$$

To solve this integral equation, we expand v in a Fourier series,

$$v(\phi)=\sum_{n=-\infty}^{\infty}v_n e^{in\phi},\quad v_n=\frac{1}{2\pi}\int_{-\pi}^{\pi}d\phi V(\phi)e^{-in\phi} \tag{37}$$

as well as $t(\phi)$. The solution of the Bethe-Salpeter equation is then simply given by

$$t(\theta)=\sum_n\frac{v_n}{1-\nu v_n}e^{in\theta}. \tag{38}$$

This expression for the Coulomb-scattering t matrix of two electrons in the Cooper channel ($\mathbf{p}_2=-\mathbf{p}_1$), in the presence of a Fermi sea, is the main result of the paper. We note that the procedure followed here is not valid for very small $r_s\ll\xi/E_F,k_BT/E_F$, which will be addressed later in Appendix B.

D. Fourier coefficients of $v(\phi)$

For the Fourier coefficients of $v(\phi)$, we integrate (37) in the complex plane with $z=e^{i\phi/2}$. We find

$$v_n=\frac{4e_0^2}{k_F\cos\gamma}\sum_{\text{odd }m\geqslant 1}^{\infty}\frac{\cos(m\gamma)}{2n+m}, \tag{39}$$

with

$$\sin\gamma=\frac{k_s}{2k_F}=\frac{r_s}{\sqrt{2}}. \tag{40}$$

For numerical estimates, it is more convenient to write the result as

$$v_n=-\frac{2e_0^2}{k_F\cos\gamma}\{\mathcal{L}_n+\mathcal{A}_n\}, \tag{41}$$

$$\mathcal{L}_n=\ln\left[\tan\left(\frac{\gamma}{2}\right)\right]\cos(2n\gamma)-\frac{\pi}{2}\sin(2n\gamma), \tag{42}$$

$$\mathcal{A}_n=2\sum_{\text{odd }m\geqslant 1}^{2n-1}\frac{\cos[\gamma(2n-m)]}{m}. \tag{43}$$

For instance, for $n=0$ we have

$$v_0=-\frac{2e_0^2}{k_F\cos\gamma}\ln\left[\tan\left(\frac{\gamma}{2}\right)\right]. \tag{44}$$

1. Integral approximation

For small r_s the sum (39) is smooth and can be approximated by an integral, giving

$$v_n \simeq \frac{2e_0^2}{k_F \cos\gamma}\left\{\sin(2n\gamma)\left[\frac{\pi}{2} - \mathrm{Si}(2n\gamma+\gamma)\right] - \cos(2n\gamma)\mathrm{Ci}(2n\gamma+\gamma)\right\}, \quad (45)$$

where Si and Ci are the sine and cosine integrals. This expression can also be obtained (for large n) with a linear expansion of the sine in $v(\phi)\simeq 2\pi e_0^2/(k_s+k_F|\phi|)$ before calculating the Fourier coefficients. For realistic parameters, it is very accurate already for $n\geqslant 1$. It yields the asymptotics for $n\gg 1$

$$v_n \simeq \frac{e_0^2}{2k_F\gamma^2\cos\gamma}\frac{1}{n^2}. \quad (46)$$

Hence, the large n dependence is polynomial, $v_n\sim n^{-2}$, which reflects the fact that the potential $v(\phi)$ is nonanalytic. This is in contrast with the 3D case, where the coefficients of the spherical harmonics decomposition are[12] $(2\pi e_0^2/k_F^2)Q_l(1+r_s^{1/2}2^{-1/4})$, and their decay is exponential in l (Q_l is the Legendre function of the second kind).

2. Small r_s approximation

We now expand (45) in small r_s and find

$$v_n \simeq -\frac{2e_0^2}{k_F}\left\{\ln(2n\gamma)+\frac{1}{2}-\pi n\gamma\right\} \to -\frac{2e_0^2}{k_F}\ln(2n\gamma). \quad (47)$$

This expression is not valid for very large n, as we expanded to lowest order in $n\gamma$. It remains finite in the limit $r_s\to 0$ because $e_0^2\sim r_s$.

IV. SCATTERING LENGTH AND EPR PAIRS

We now apply our result to a realistic GaAs 2DEG and study the dependence of the scattering amplitude on the scattering angle θ, on r_s, and on temperature, before discussing the production and detection of spin-entangled electron pairs.

A. The different scattering lengths

We define the scattering length for singlets and triplets

$$\lambda_{S/T}(\theta) = |f(\theta) \pm f(\theta-\pi)|^2, \quad (48)$$

following (16). We recall the scattering amplitude $f(\theta)$ defined in (6),

$$f(\theta) = \frac{m}{\hbar^2\sqrt{2\pi k_F}}t(\theta), \quad (49)$$

with the t matrix given by (38). Unpolarized sources contain $1/4$ of singlets and $3/4$ of triplets [see Eq. (4)], which yields the scattering length

$$\lambda(\theta) = \tfrac{1}{4}\lambda_S(\theta) + \tfrac{3}{4}\lambda_T(\theta). \quad (50)$$

We also define the scattering length $\lambda^{(1)}$ obtained from the Born approximation with the amplitude

$$f^{(1)}(\theta) = \frac{m}{\hbar^2\sqrt{2\pi k_F}}v(\theta), \quad (51)$$

as well as the corresponding bare scattering lengths λ_C and $\lambda_C^{(1)}$, obtained by replacing $t(\theta)$ with $t_C(\theta)$ and $v_C(\theta)$, given by Eqs. (8) and (7). We point out that $\varsigma = r_s/\sqrt{2}$.

B. Total scattering length

We now take typical parameters for a 2D GaAs electron gas,[37] $\epsilon_r=13.1$, $r_s=0.86$, and a sheet density $n=10^{15}\ \mathrm{m}^{-2}$, and assume $\xi < k_BT = 10^{-2}E_F$ ($T=20$ mK). First, we estimate the magnitude of the scattering and calculate the total scattering length integrated over π

$$\lambda_{\mathrm{tot}} = \int_0^\pi d\theta\lambda(\theta) = \tfrac{1}{4}\lambda_S^{\mathrm{tot}} + \tfrac{3}{4}\lambda_T^{\mathrm{tot}} = 3.39\ \mathrm{nm}, \quad (52)$$

with

$$\lambda_S^{\mathrm{tot}} = 7.92\ \mathrm{nm}, \quad \lambda_T^{\mathrm{tot}} = 1.88\ \mathrm{nm}. \quad (53)$$

This is consistent with the ladder approximation, which requires $\lambda_{\mathrm{tot}}k_F = 0.54 < 1$. We now use the Born approximation (51) and write $\lambda_{\mathrm{tot}}^{(1)} = \lambda_{\mathrm{dir}}^{(1)} - \lambda_{\mathrm{ex}}^{(1)}$. We find for the direct part

$$\lambda_{\mathrm{dir}}^{(1)} = \int_0^{2\pi} d\theta|f(\theta)|^2 = \lambda_F\frac{\tan\gamma}{\cos\gamma}\left\{1 - 2\sin\gamma\tan\gamma \times \mathrm{arctanh}\left(\sqrt{\frac{1-\sin\gamma}{1+\sin\gamma}}\right)\right\} \quad (54)$$

with the Fermi wavelength $\lambda_F = 2\pi/k_F$, and we recall that $\sin\gamma = r_s/\sqrt{2}$. The exchange term is

$$\lambda_{\mathrm{ex}}^{(1)} = \mathrm{Re}\int_0^\pi d\theta f(\theta)f(\theta-\pi) = \lambda_F\frac{\sin^2\gamma}{\cos 2\gamma}\left\{\log\left(\sin\gamma + \frac{1}{\sin\gamma}\right) - \tan\gamma\,\mathrm{arctanh}(\cos\gamma)\right\}, \quad (55)$$

which yields $\lambda_{\mathrm{total}}^{(1)} = 11.0$ nm. We see here that the Born approximation significantly overestimates the exact result (52). For small r_s, we can further approximate $\lambda_{\mathrm{dir}}^{(1)} \simeq \lambda_F r_s/\sqrt{2}$ and $\lambda_{\mathrm{ex}}^{(1)} \simeq (\lambda_F r_s^2/2)\log(\sqrt{2}/r_s)$, which gives an even greater length, $\lambda_{\mathrm{tot}}^{(1)} \simeq 17.2$ nm. In the limit $r_s\to 0$, the strength of the Coulomb interaction $e_0^2 \propto r_s$ also vanishes. As a consequence, the cross section remains finite—despite the forward-scattering ($q=0$) divergence of the unscreened Coulomb potential.

C. Angular dependence

We compare in Fig. 4 the angular dependence of the different scattering lengths for unpolarized electrons. We first see that the main effect of the Fermi sea is to reduce significantly the scattering by one order of magnitude compared to the vacuum case. The large renormalization is related to the relatively large value of $r_s=0.86$ (and the large screening

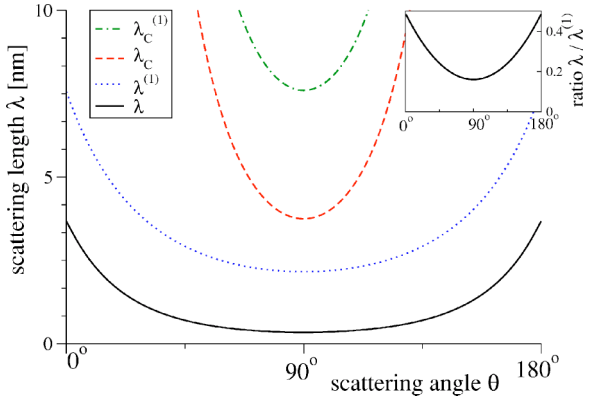

FIG. 4. Scattering length $\lambda(\theta)$ for a GaAs 2DEG with sheet density $n=4\times10^{15}$ m^{-2} and $k_BT=E_F/100=2$ K, for unpolarized incident electrons. We compare the exact result (50) for a 2D Fermi gas to its Born approximation $\lambda^{(1)}$, and to the bare scattering result (with no screening) λ_C and $\lambda_C^{(1)}$ [see Eq. (51)]. The main effects of the many-body background is to remove the $\theta=0$ divergence by screening the Coulomb interaction and to significantly reduce the Born approximation via the logarithmic corrections in Eq. (38). The inset shows the ratio of the exact scattering length $\lambda(\theta)$ to the Born approximation result $\lambda^{(1)}$.

$k_s\sim k_F$), which strongly reduces the forward-scattering divergence of the bare scattering $\lambda_C,\lambda_C^{(1)}(\theta\to0)$. Furthermore, we notice that the Born approximation $\lambda^{(1)}$ is not valid in the Cooper channel, as higher-order terms reduce the scattering amplitude. The fact that higher terms contribute significantly, despite the weakness of $V(q)$, is due to their logarithmic enhancement by the factor ν.

The angular dependence of the exact scattering length λ is similar, but not identical to the Born approximation result $\lambda^{(1)}$, as shown in the inset of Fig. 4. Importantly, $\lambda(\theta)$ is a smooth, monotonic (for $\theta<\pi/2$) function, so that the interference mechanism survives for the production of EPR pairs at $\theta=\pi/2$.

D. r_s dependence and Born approximation

We show in Fig. 5 a plot of the scattering length as a function of the density n or $r_s=me_0^2/\hbar^2\sqrt{\pi n}$ (top axis; we keep e_0 constant), for the angle $\theta=\pi/2$ (hence, only the singlet channel contributes). There is a strong dependence $\sim n^{-1}$ of the scattering, which could be studied experimentally by varying n via a top gate. This dependence also roughly applies to $\lambda^{(1)}$ and λ_C, while $\lambda_C^{(1)}\sim V_C^2/k_F\sim n^{-3/2}$.

The Born approximation $t(\theta)\simeq v(\theta)$ is reached when the logarithmic factor disappears ($\nu\to0$) and does not enhance higher-order terms [see Eq. (38)]. This occurs at high temperatures $k_BT\to E_F$, for hot electrons $\xi\simeq E_F$, or for electrons that are not in the Cooper channel ($P\simeq k_F$). The Born approximation is also reached in the very small $r_s\sim0.01$ limit (not shown), when $\nu v_n\ll1$. For even smaller r_s one can neglect k_s in V, which yields the Born approximation of the bare Coulomb potential $t\simeq V_C$. We note that the effect of the Fermi sea is intrinsic in our calculation (by restricting the intermediate states to the Fermi surface), which, therefore,

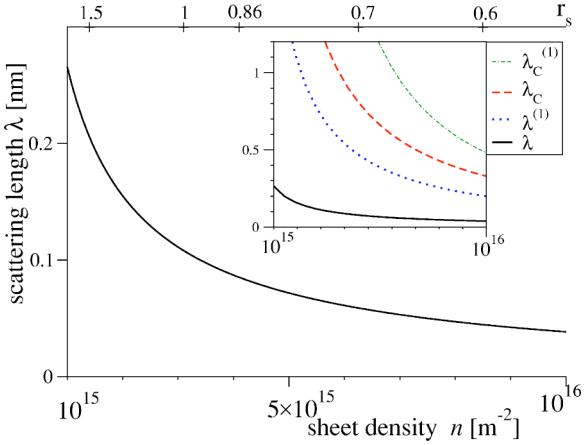

FIG. 5. Scattering length λ at $\theta=\pi/2$ as a function of the density n (see the corresponding $r_s=me_0^2/\hbar^2\sqrt{\pi n}$ on the top axis). The inset shows the comparison with the Born approximation and the bare scattering.

cannot recover in the $r_s\to0$ limit the exact result for the bare Coulomb interaction (8).

E. Dependence on T, ξ, and α

Two effects appear when one varies the temperature T, the excitation energy ξ of the incident electrons or the impact angle $\alpha=\angle(\mathbf{p}_1,-\mathbf{p}_2)/2$ (a finite $|p_1-p_2|$ plays the same role). The first one is a change in the factor ν appearing in the denominator $1-\nu v_n$ of the t matrix (38). For finite α, one should, in principle, integrate $\nu(\phi)=(m/2\pi\hbar^2)\log(2\alpha\sin|\phi|)$ over the intermediate angle $\phi=\angle(\mathbf{k},\mathbf{p})$ in the Bethe-Salpeter equation $t(\phi)=v(\phi)+(1/2\pi)\int d\phi\nu(\phi)v(\phi)t(\phi)$. However, the dependence of $\nu(\phi)$ is smooth (logarithmic) compared to the behavior of the Coulomb potential at the Fermi surface, $v(\phi)\sim1/(\phi+r_s\sqrt{2})$. Therefore, we neglect this dependence and set, e.g., $\phi\simeq\pi/3$ in $\nu(\phi)$, which gives a constant $\nu\simeq(m/2\pi\hbar^2)\log(\alpha)$. Hence, we take

$$\nu=\frac{m}{2\pi\hbar^2}\log\left(\max\left\{\frac{\xi}{E_F},\frac{k_BT}{E_F},\alpha\right\}\right). \tag{56}$$

The effect of this dependence on the scattering length λ at $\theta=\pi/2$ is shown in Fig. 6. In Fig. 6(a) we fix $\xi/E_F=10^{-3}$, $k_BT/E_F=10^{-2}$ and vary α (we recall that the Fermi temperature is $E_F/k_B=162$ K). First, λ is constant when $\alpha<k_BT/E_F$ and then increases slowly (the horizontal scale is logarithmic) as ν decreases; for $\alpha\to1\Rightarrow\nu\to0$, we recover the Born approximation $\lambda^{(1)}$. The function λ is exactly the same if one interchanges ξ and k_BT [Fig. 6(b)] or permutes all the three parameters ξ, k_BT, and α [Figs. 6(c)–6(f)].

Second, we take into account the requirement that the outgoing states $\mathbf{p}'_{1,2}$ are not occupied (and, hence, available for the outgoing scattering states), by introducing the factor $F=[1-n(\xi'_1)][1-n(\xi'_2)]=n(-\xi'_1)n(-\xi'_2)$, plotted in Fig. 6 (right vertical axis). At $\theta=\pi/2$ we have $p'_{1,2}=p_1(\cos\alpha\pm\sin\alpha)\Rightarrow\xi'_{1,2}=\xi\pm E_F\sin(2\alpha)$ [see Fig. 1(c)]; hence, for a large α the final state $\xi'_2<0$ will be already

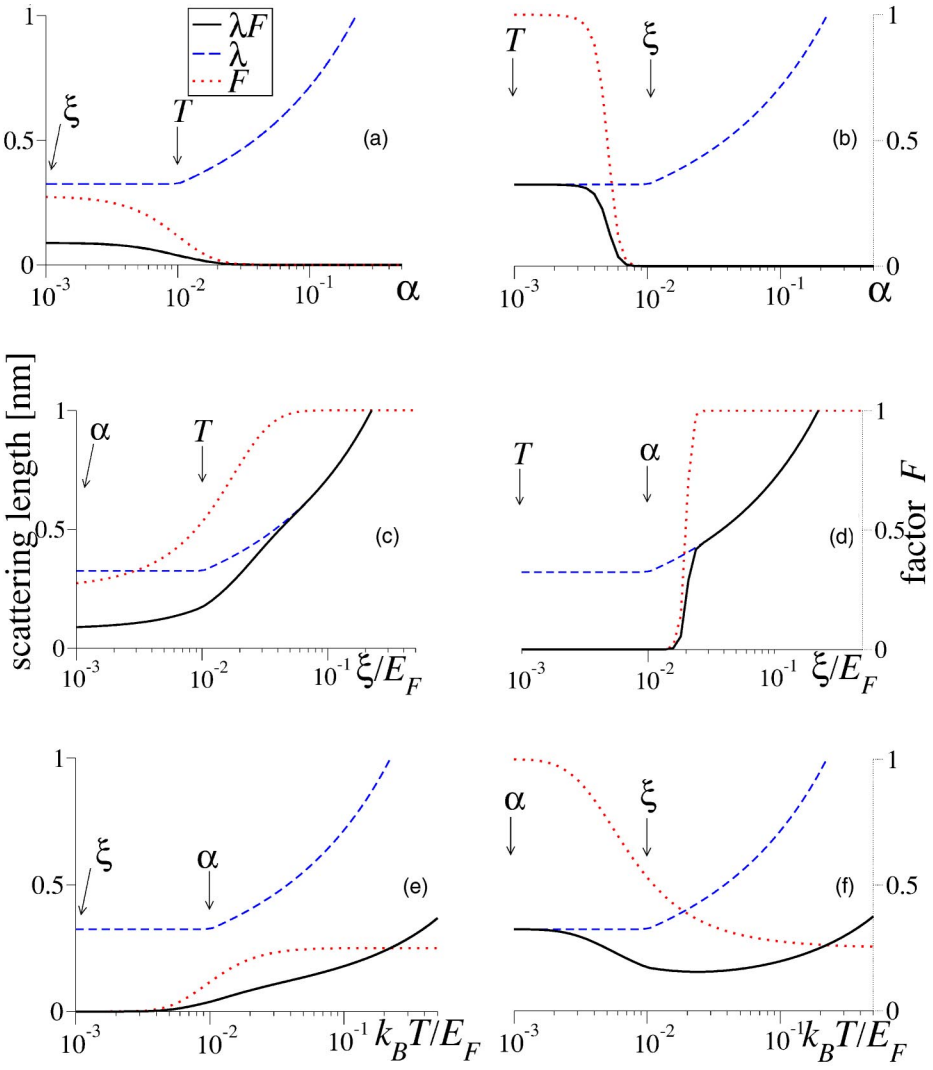

FIG. 6. "Observational" scattering length λF at $\theta=\pi/2$ as a function of the impact angle α [(a) and (b)], the excitation energy ξ [(c) and (d)], and temperature T [(e) and (f)] (left axis). The Fermi occupation factor $F=[1-n(\xi_1')][1-n(\xi_2')]$ (right axis) enforces the requirement that the outgoing states $\xi_{1,2}'=\xi\pm E_F\sin(2\alpha)$ are available for the outgoing scattering states. The dependence of the "bare" λ comes from ν (56) and is the same in all graphs. The arrows indicate the position of the fixed values, e.g., $\xi/E_F=10^{-3}$, $k_BT/E_F=10^{-2}$ (a), $\xi/E_F=10^{-2}$, $k_BT/E_F=10^{-3}$ (b), etc.

occupied and the scattering into this channel will be prohibited. The transition across the Fermi surface always occurs at the largest quantity [e.g., at $k_BT\gg\xi$ in Fig. 6(a)] and is sharp when temperature is negligible [Figs. 6(b)–6(d)]. Note that here we consider that the initial states $\mathbf{p}_{1,2}$ are always filled (i.e., with occupation 1), being either injected from the QPC or thermally excited.

In Fig. 6(a) the maximum value of F (when $\alpha E_F\ll k_BT$) is $F=1/4$ because the final energies $|\xi_{1,2}'|\ll k_BT$ lie within the temperature window $n(0)=1/2$. The same occurs in Fig. 6(c) for $\xi\ll k_BT$, while $F=1$ for $\xi\gg k_BT$. For negligible temperature [Figs. 6(b) and 6(d)] F saturates to 1 when $\alpha E_F\ll\xi$. We finally note that (for the factor F), Fig. 6(e) corresponds to the opposite of Figs. 6(a) and 6(f) is opposite of 6(c) and 6(b) is opposite of 6(d).

We can now consider the combined effect of λ and F by defining the "observational" scattering length λF, giving the scattering length as could be measured in a real experiment. As a function of α, it only reproduces F by showing a smooth 6(a) and sharp 6(b) step. In Fig. 6(c), it first increases slowly because of the smooth transition from $F=1/4\to1$ in the region of constant λ (small ξ), before following the logarithmic increase of λ (large ξ). In Fig. 6(d) the transition is sharp and starts at $\lambda F=0$. In Fig. 6(e), the transition is smooth, and the measurable length λF follows λ but is reduced by a factor of 4. In Fig. 6(f), there is an interesting nonmonotonic behavior in the region above $k_BT/E_F>\alpha$; however, it requires an extremely small α, e.g., $\alpha\simeq0.2°$, not reachable in a realistic experiment. We note that the rightmost parts of the graphs (above 10^{-1}) are only indicative because they do not correspond to regime assumed in the derivation of λ ($k_BT/E_F,\xi/E_F,\alpha\ll1$).

The scattering length vanishes logarithmically, $\lambda\sim1/\log(\nu V)\to0$ when all k_BT, ξ, and $\alpha\to0$. It is reminiscent of the vanishing of the inverse lifetime of a single quasiparticle excitation scattering with other electrons below the Fermi surface, when its excitation energy vanishes.[7] However, the two cases are completely different: the lifetime diverges because of phase-space constraints due to the Fermi statistics; in our case, the scattering of two particles *above* the Fermi sea vanishes because of the renormalization due to the Fermi sea.

F. Quantum oscillations

In addition to the destructive and constructive interference at $\theta=\pi/2$, quantum oscillations can be seen in the *bare* scat-

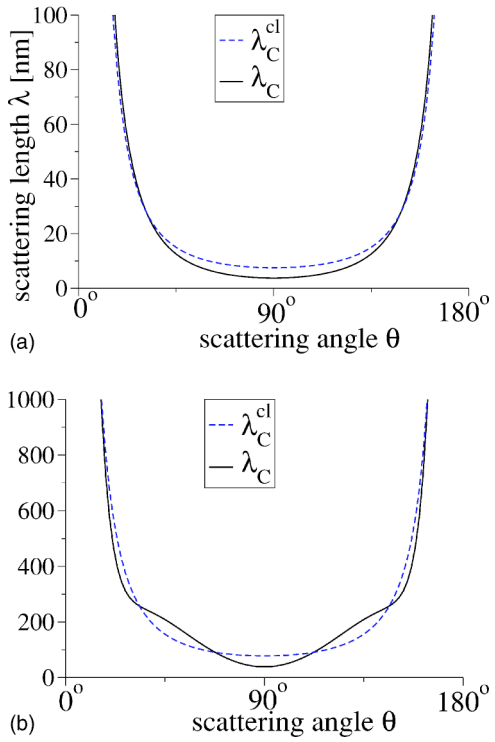

FIG. 7. Scattering length for the bare Coulomb interaction [given by Eq. (8)] compared to the classical value given by $\lambda_C^{\rm cl}=|f_C(\theta)|^2+|f_C(\theta-\pi)|^2$: (a) $\varsigma=0.6$ corresponding to $n=4\times10^{15}$ m^{-2} and (b) $\varsigma=2$ ($n=4\times10^{14}$ m^{-2}).

tering (of singlets, triplets, or unpolarized sources) as a consequence of the angle-dependent phase $\varsigma\ln|\sin\theta/2|$ appearing in Eq. (8). The number of oscillations is roughly given by $\varsigma=r_s/\sqrt{2}$, as illustrated in Fig. 7. We see that the oscillations are absent for $n=4\times10^{15}$ m^{-2} and only appear at lower density. At $\theta=\pi/2$, the quantum amplitude for unpolarized sources is half of the classical one given by $\lambda_C^{\rm cl}=|f_C(\theta)|^2+|f_C(\theta-\pi)|^2$ because the triplet contribution vanishes.

For the many-particle result, such quantum oscillations could arise from the small imaginary part appearing with the logarithm in $\nu(T)=(m/2\pi\hbar^2)[\ln(k_BT/E_F)+(\pi/2)i]$, as it yields an angle-dependent phase when summing up the Fourier series. However, the phase is of the order $1/\ln(k_BT/E_F)\ll1$, and the oscillations are not visible.

G. Production of EPR pairs

We now consider the setup of Fig. 1(b) with detectors placed at an angle $\theta\simeq\pi/2$. The triplet channel is nonzero because of the small aperture angle $2\delta\theta$ of the detectors. The scattering lengths for the singlet and triplet channels into the detectors read

$$\bar{\lambda}_{S/T}(\theta,\delta\theta)=2\int_{\theta-\delta\theta}^{\theta}d\theta'|f(\theta')\pm f(\pi-\theta')|^2, \tag{57}$$

which we use to define the ratio

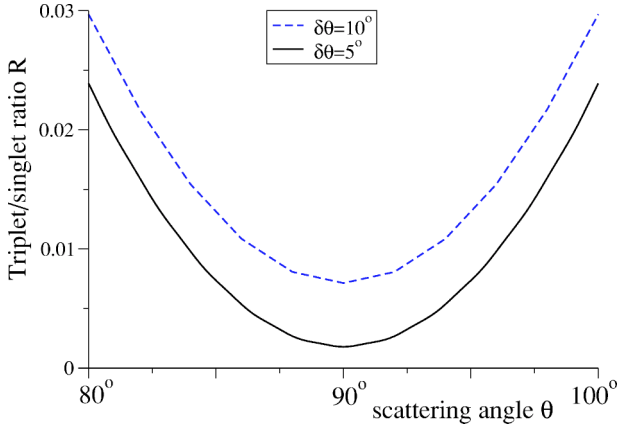

FIG. 8. Ratio $R(\theta\delta\theta)$ of the number of triplets and singlets collected in the detectors, placed at an angle θ and with an aperture $\delta\theta=5°,10°$.

$$R(\theta,\delta\theta)=\frac{N_T}{N_S}=\frac{3\bar{\lambda}_T}{\bar{\lambda}_S} \tag{58}$$

between the number $N_{T/S}$ of singlet and triplets collected in the detectors. Here we have allowed for the case where the average scattering angle θ deviates from $\pi/2$. We show a plot of $R(\theta,\delta\theta)$ in Fig. 8 for $\delta\theta=5°$ and 10°. We find very low values, $R(90°,5°)=0.183\%$ or $R(85°,5°)\simeq R(90°,10°)\simeq0.7\%$, which shows that the collision entangler is efficient because singlets are predominantly collected in the detectors, even for $\theta=80°$. We note that such a deviation from $\pi/2$ would occur experimentally because the electrons injected through the QPCs have an angular spread. This spread could, however, be reduced by the use of a lense-shaped top gate implementing a refractive medium for the electron motion.[2]

Expanding in $\delta\theta$ we find

$$\bar{\lambda}_{S/T}(\theta,\delta\theta)\simeq2\delta\theta(f\pm f_{\rm ex})^2+\frac{2}{3}\delta\theta^3[(f'\mp f'_{\rm ex})^2-(f\pm f_{\rm ex})(f''\pm f''_{\rm ex})]+\mathcal{O}(\delta\theta^4) \tag{59}$$

with

$$f\equiv f(\theta),\quad f_{\rm ex}\equiv f(\theta-\pi) \tag{60}$$

and $'$ denotes $d/d\theta$. For $\theta=90°$, $\delta\theta=5°$, and neglecting f'' we get

$$R(90°,\delta\theta)=\left|\frac{f'(\pi/2)}{f(\pi/2)}\right|^2\delta\theta^2=0.178\,\%\,, \tag{61}$$

which is close to the exact value $R=0.183\%$ found above. Thus the Taylor approximation is accurate, and it is clear that the triplet contribution can be made arbitrarily small by reducing the aperture $\delta\theta$. We note that our calculation gives a ratio $|f'/f|$ of the order unity for a wide range of parameters, $k_BT/E_F=10^{-1}-10^{-10}$ and $r_s=0.1-1$. Using the Born approximation we find a significantly lower value ($\delta\theta=5°$)

$$R(90°, \delta\theta) \simeq \frac{1}{4(r_s+1)^2}\delta\theta^2 = 0.05\,\%\,, \tag{62}$$

which would be more advantageous for EPR production (see the discussion on hot electrons in Sec. IV I).

H. Current

We now estimate the singlet current collected in the detectors for a given input current I. We neglect the angular dispersion of the incident electrons (due to diffraction on the edge of the QPC) by assuming that the electrons occupy the lowest transverse mode in the QPC, and that the remaining spread could, in principle, be compensated by the use of a lensing effect.[2] This gives longitudinal plane waves (with wave vectors $\mathbf{p}_{1,2}$) having a transverse width w roughly given by half the width of the QPC.

We first note that the scattering length for the singlet channel is small, $\overline{\lambda_S}=0.24$ nm. Taking $w=100$ nm, we find the probability

$$P_S = \frac{1}{4}\frac{\overline{\lambda_S}}{w} = 0.06\% \tag{63}$$

for the singlets to be scattered into the detectors. First, we assume that the electrons are injected simultaneously from the reservoirs, which can be achieved by opening and closing both QPCs at the same time. This yields a singlet current of

$$I_S = P_S I = 0.6 \text{ pA}. \tag{64}$$

We have considered a given current of $I=1$ nA, which corresponds to a frequency in the GHz range for the opening and closing of the QPCs. Otherwise, the electrons are injected at random times, given by a Poisson process with rate $W_{\text{in}}=e/I$. Then the probability of finding two electrons inside the scattering region (i.e., in state $|\mathbf{p}_1,\mathbf{p}_2\rangle$) is roughly $P_{12}=(W_{\text{out}}/W_{\text{in}})^2$, where W_{out} is the rate of escape from the scattering region into the drain contacts (Fig. 1). Finally, we find the *total* scattering probability of two electrons

$$P_{\text{tot}} = \frac{\lambda_{\text{tot}}}{w} = 3.4\% \tag{65}$$

(i.e., not necessarily into the detector).

An additional interesting topic is the noise[41] of the detected current. As this is outside the scope of the present work, we only present heuristic arguments. As the scattering probability is very small, one can assume that subsequent pairs do not interact with each other. This implies that the zero-frequency noise induced by the scattering should be mainly given by the partition noise

$$S(\omega=0) \propto IP_S(1-P_S) \simeq IP_S,$$

which becomes Poissonian for $P_S \ll 1$. The pulsed injection of the electron via, e.g., the periodic lowering of the QPC barriers, reduces the stochastic nature of the tunneling through the QPC if the lowering is sufficiently fast. On the other hand, this periodic change should lead to a more complex noise behavior for finite frequencies.[42]

I. Hot electrons

It is interesting to consider the case of hot electrons with larger excitation energies ξ (e.g., a fraction of the Fermi energy E_F of the scattering region), obtained by applying a dc bias voltage ΔV across the input QPCs. It can be problematic to have incident electrons with such a wide range of energy as this allows a mismatch of the incident energies ($\xi_1 \neq \xi_2$) after averaging over both incident energy ranges, which introduces uncertainties in the scattering angle (see Fig. 1). To avoid this situation, one can raise the QPC heights such as to allow only a very small range of electrons to go above the QPC barrier.[2] For hot electrons with $\xi \simeq E_F$, the exact result moves toward the Born approximation [see Eq. (62) and Fig. 4]. Hence, the scattering length increases [because the logarithmic factor decreases $\nu \sim \log(\xi/E_F)$], while the triplet/singlet ratio becomes more favorable (i.e., smaller). On the other hand, the scattering length becomes smaller for higher momentum [as $V \sim 1/(k+k_s)$]. Taking, e.g., $e\Delta V=3$ meV $\simeq E_F/5^2$, one finds values that are more favorable than for cold electrons: the singlet length is doubled $\overline{\lambda_S^{(1)}}=0.56$ nm, while the triplet/singlet ratio is halved $\mathcal{R}=0.10\%$. Note that hotter electrons have a smaller lifetime because of the increased phase space that is available for scattering with electrons below the Fermi surface.[7] Estimates of the electron-electron scattering length $l_{e\text{-}e}$ have been obtained[2] for a GaAs 2DEG using imaging techniques via an SPM, in good agreement with theoretical predictions.[7] In our case, one has $l_{e\text{-}e} \simeq 1.2\ \mu$m, which is similar to the scale $L \simeq 1\ \mu$m of our envisioned setup. Hence, one can expect some reduction of the signal due to relaxation into the Fermi sea, roughly given by $\sim e^{-L/l_{e\text{-}e}} \sim 0.3$.

J. Detection of entanglement

An important question is to demonstrate that the collected electrons are indeed spin-entangled EPR pairs. We propose here three ways to answer this question experimentally. The first one is to refocus the scattered electrons into a beam splitter and carry out noise measurements in one outgoing lead; in this situation enhanced noise (bunching) is a signature of the desired singlet state, while zero noise corresponds to entangled or unentangled triplets.[43] However, this method would probably require some bridges to avoid the source reservoirs. The second one is to carry out tests of violation of Bell inequality,[28,44,45] by measuring single-spin projections via a single-electron transistor coupled to a spin-filtering device. The latter can be a quantum dot in the Coulomb blockade regime[46] or a QPC (Ref. 47) in a strong in-plane magnetic field. The third method consists in adding a *p-i-n* junction,[48,49] allowing the recombination of the entangled electrons with unentangled holes into photons; one should then carry out the test of the Bell inequality with the photons, by measuring their entangled polarization modes.

In addition, we mention that the interference mechanism responsible for the vanishing of the triplets at $\pi/2$ could be demonstrated by polarizing the incoming electrons spin, which can be achieved by applying a large in-plane magnetic field to turn the QPCs into spin filters,[47] or by replacing them with quantum dots.[46] The current recorded at the detectors,

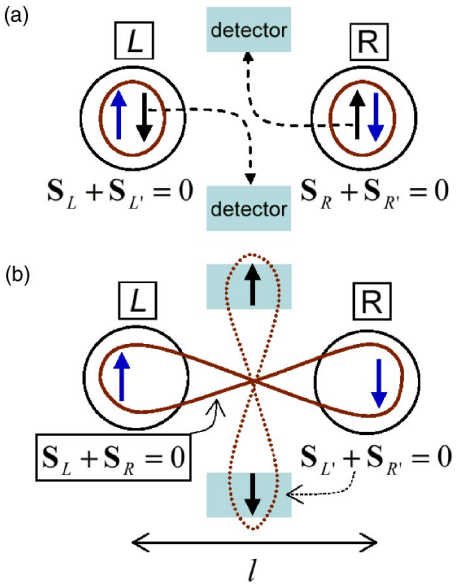

FIG. 9. Creation of nonmobile entanglement. Each input QPC is replaced by a quantum dot (L and R) containing two excess electrons. The ground state in each dot is the singlet with total spin $\mathbf{S}_L+\mathbf{S}_{L'}=\mathbf{S}_R+\mathbf{S}_{R'}=0$ (a). One injects one electron from each dot (e.g., L' and R'), and allows them to scatter. When they are detected at a $\pi/2$ scattering angle, we know that they are in the singlet state $\mathbf{S}_{L'}+\mathbf{S}_{R'}=0$ (b). As the total spin is conserved, the two remaining electrons in dots L and R are also in the singlet state $\mathbf{S}_L+\mathbf{S}_R=0$ and, therefore, form a localized EPR pair whose members are separated by the interdot distance l.

which is proportional to the fraction of incoming singlets $\rho_S=(1-\mathcal{P}^2)/2$, should then rapidly decrease as the polarization $\mathcal{P}$ of the spins increase.

K. Creation of localized, nonmobile entanglement

In this section, we discuss a way to produce static spin-entangled electrons, described in Fig. 9. We propose to replace the two "injection" QPCs with two quantum dots, each with an even number of electrons, so that two excess electrons are in the singlet ground state.[50] Lowering the tunneling barrier defining the dots allows for the simultaneous injection of one electron (of the singlet pair in each dot) into the scattering region. If these electrons are detected at $\pi/2$ by the detector, then we know that they must be in a spin-singlet state (with certainty $1-N_T/N_S$). As spin is conserved during the Coulomb scattering, the total spin for the two electrons left in the two dots must be zero, which corresponds to the spin-singlet state. Therefore, one has created a localized (nonmobile) entangled pair of electrons separated by an interdot distance $l\sim 1$ μm. This instantaneous "creation" (obtained by postselection) is a dramatic illustration of Einstein's "spooky action at a distance." Contrary to the standard EPR paradox, it does not manifest itself in the results of measurement correlations, but in the "creation" of a nonlocal (in the sense of nonoverlapping wave functions) quantum state. Such a process, similar in some sense to entanglement swapping or quantum teleportation, could be useful in a scalable quantum computer to create entangled pairs without having to go through the standard sequence of swapping state, which requires moving one electron to neighboring site of the other one, entangling them by local interaction,[18] and moving the electron back to its original place. However, we note that our scheme requires a large number of collisions, of the order of $1/P_S$; this number scales fortunately more slowly ($\sim 1/\delta\theta$) with the aperture $\delta\theta$ than the precision ($\sim N_S/N_T\sim 1/\delta\theta^2$).

V. ELECTRON-PHONON AND ELECTRON-ELECTRON INTERACTION

In this section we investigate the question of whether phonons can influence the scattering amplitude in a significant way. We first note that the scattering of electrons on real phonons can be neglected here, as it is strongly suppressed at low temperature. This is illustrated, for instance, by the absence of phonon effects in the experiments of Refs. 1 and 2. However, the effective electron-electron interaction arising from the exchange of virtual phonons does not depend on temperature, so that it could play a role in the electron-electron scattering. Our goal here is to estimate it and compare it to the screened Coulomb interaction that we have considered thus far. We shall see that the contribution of acoustic phonons (deformation and piezoelectric coupling) is negligible, while the polar phonons give a smooth monotonic decrease of the electron-electron interaction that is less than 20%, and as such does not change qualitatively the results presented in Sec. IV.

A. 2D phonon-mediated electron-electron interaction

In 3D, the effective electron-electron interaction is given by[5]

$$H_{e\text{-}e}^{\mathrm{ph}}=\frac{1}{2V}\sum_{\vec{k},\vec{k}'}\sum_{\vec{q}}c_{\vec{k}+\vec{q}}^{\dagger}c_{\vec{k}'-\vec{q}}^{\dagger}c_{\vec{k}'}c_{\vec{k}}W^{\mathrm{ph}}(\vec{q}), \tag{66}$$

where V is the normalization volume, $\vec{q}=(\mathbf{q},q_z),\vec{k},\vec{k}'$ are 3D vectors, and $\mathbf{q},\mathbf{k},\mathbf{k}'$ are 2D vectors in the plane of the 2DEG (in the following we keep the notation $q=|\mathbf{q}|$). The electron-electron interaction matrix element reads

$$W^{\mathrm{ph}}(\vec{q})=|M(\vec{q})|^2\frac{2}{\hbar V}\frac{\omega_{\mathrm{ph}}(q)}{\omega^2-\omega^2(q)}, \tag{67}$$

where $\omega_{\mathrm{ph}}(q)$ is the phonon dispersion and $M(\vec{q})$ is the matrix element for the electron-phonon interaction

$$H_{e\text{-ph}}=\frac{1}{V}\sum_{\vec{q}}\sum_{\vec{k}\sigma}c_{\vec{k}+\vec{q},\sigma}^{\dagger}c_{\vec{k}\sigma}(b_{\vec{q}}+b_{-\vec{q}}^{\dagger})M(\vec{q}). \tag{68}$$

Here $b_{\vec{q}}^{\dagger}$ and $c_{\vec{k}}^{\dagger}$ are phonon and electron creation operators. We shall consider the lowest order in W^{ph}, which in the Cooper channel allows us to take the static limit $\omega=0$ as all the energies involved in the scattering are the same, $E_i\simeq E_F$.

The electron-phonon interaction $M(\vec{q})$ as well as the effective interaction $W^{\mathrm{ph}}(\vec{q})$ are always 3D as they involve coupling of the 2D electrons with the bulk 3D phonons. There is no 3D screening of the bare ion-electron Coulomb interac-

tion, as there are no mobile charges in the bulk. Now we define an effective 2D interaction $W_{2D}(\mathbf{q})$, which we shall compare to the unscreened 2D Coulomb interaction V_C. We assume that the electron wave function is separable into a plane wave $|\mathbf{k}\rangle$ and a confined lateral function $|\psi\rangle$. For instance, one can take an infinite square well of width L

$$\psi(z) = \frac{2}{L}\sin\left(\frac{\pi z}{L}\right), \tag{69}$$

which yields the width of the 2DEG

$$d = \langle z^2 - \langle z^2\rangle\rangle^{1/2} = L\sqrt{\frac{1}{2\pi^2} - \frac{1}{6}} \simeq 0.18L. \tag{70}$$

We prefer to consider the alternative variational solution of the triangular well present at the interface,[37]

$$|\psi(z)|^2 = \tfrac{1}{2}\kappa^3 z^2 e^{-\kappa z} \tag{71}$$

with the width

$$d = \frac{\sqrt{3}}{\kappa}, \tag{72}$$

as it allows for simple analytical expressions. We define the effective $W_{2D}^{\mathrm{ph}}(\mathbf{q}=\mathbf{k}-\mathbf{k}')$ by

$$\langle \mathbf{k}_1', \psi; \mathbf{k}_2', \psi | W^{\mathrm{ph}} | \mathbf{k}_1, \psi; \mathbf{k}_2, \psi\rangle = \delta(\mathbf{k}_1 + \mathbf{k}_2 - \mathbf{k}_1' - \mathbf{k}_2') W_{2D}^{\mathrm{ph}}(\mathbf{q}) \tag{73}$$

and get[15]

$$W_{2D}^{\mathrm{ph}}(\mathbf{q}) = \int dz \int dz' |\psi(z)|^2 |\psi(z')|^2 W^{\mathrm{ph}}(\mathbf{q}; z - z')$$

$$= \frac{1}{2\pi}\int dq_z W^{\mathrm{ph}}(\mathbf{q}, q_z) |I(q_z)|^2, \tag{74}$$

with $W^{\mathrm{ph}}(\mathbf{q},z) = (1/2\pi)\int dq W^{\mathrm{ph}}(\mathbf{q},q_z)e^{-iqz}$ and the form factor

$$I(q_z) = \int dz e^{iq_z z} |\psi(z)|^2. \tag{75}$$

The latter is particularly simple for the triangular well, $I(q_z) = (iq_z/\kappa - 1)^{-3}$. Our goal is to find the strength of this additional *e-e* interaction relative to the unscreened Coulomb potential V_C, by defining the ratio

$$r = \frac{W_{2D}^{\mathrm{ph}}}{V_C}(q = k_F). \tag{76}$$

Parameters for GaAs. We consider a well of width $d = 5$ nm, and take the following parameters[51] for GaAs: the mass density $\rho_m = 5320\ \mathrm{kg/m^3}$, the deformation potential constant $D = -7$ eV, the piezoelectric constant $eh_{14} = 1.44 \times 10^9$ eV/m, the acoustic sound velocity $c = 3700$ m/s (we assume here that c is the same for both longitudinal and transverse phonons), the optical (longitudinal and transverse) phonon frequencies $\hbar\omega_{LO} = 36.6$ meV, $\hbar\omega_{TO} = 33.8$ meV, the ionic plasmon frequency $\Omega_{p,i} = 85.5$ meV, and, finally, the low- and high-frequency dielectric constants $\epsilon(0) = 12.9$, $\epsilon(\infty) = 10.89$.

B. Acoustic phonons: Coupling to the deformation potential

We first consider electrons coupled to the acoustic phonons via the deformation potential. The electron-phonon matrix element is[52]

$$M(\vec{q}) = D\sqrt{V\frac{\hbar}{2\rho_i c}|\vec{q}|}. \tag{77}$$

where D is the deformation constant, ρ_i is the mass density, and the dispersion relation is $\omega_{\mathrm{ph}}(\vec{q}) = c|\vec{q}|$. The static effective *e-e* interaction is a constant

$$W^{\mathrm{ph}}(\vec{q}) = -\frac{D^2}{\rho_i c^2}, \tag{78}$$

which yields in 2D for the triangular well (71)

$$W_{2D}^{\mathrm{ph}}(\mathbf{q}) = -\frac{D^2}{\rho_i c^2}\frac{3\kappa}{16}. \tag{79}$$

The ratio (76) becomes

$$r(q) = -q\frac{D^2}{\rho_i c^2 e^2}\frac{3\sqrt{3}}{16d} \overset{q=k_F}{=} -1.4\times 10^{-3}, \tag{80}$$

which shows that the effective interaction W_{2D}^{ph} can be neglected for deformation potential coupling.

C. Acoustic phonon: Piezoelectric coupling

For piezoelectric coupling, the matrix element reads[52]

$$M(\vec{q}) = \frac{eh_{14}}{\epsilon_r}\sqrt{V\frac{\hbar}{2\rho_i\omega_{\mathrm{ph}}(q)}A(\vec{q})}, \tag{81}$$

with the polarization constant eh_{14} and the anisotropy factor

$$A(\vec{q}) = \begin{cases} 9q_z^2 q^4/2|\vec{q}|^6 & (LA) \\ (8q_z^4 q^2 + q^6)/4|\vec{q}|^6 & (TA) \end{cases} \tag{82}$$

for longitudinal (LA) or transverse (TA) phonons. It can be replaced by $A_{\mathrm{LA}} = 0$, $A_{\mathrm{TA}} = 1/4$ for a 2D system constraining momentum transfers to $q_z = 0$. This gives

$$M_q = \frac{eh_{14}}{\epsilon_r}\sqrt{V\frac{\hbar}{8\rho_i c|\vec{q}|}}. \tag{83}$$

The static *e-e* interaction is therefore proportional to the 3D Coulomb interaction,

$$W^{\mathrm{ph}}(\vec{q}) = -\frac{1}{\rho_i}\left(\frac{h_{14}}{2c\epsilon_r}\right)^2\frac{e^2}{q^2}. \tag{84}$$

Performing the transformation (74), we find for small $q \lesssim k_F/10$ the effective 2D potential

$$W_{2D}^{\mathrm{ph}}(\mathbf{q}) = -\frac{1}{\rho_i}\left(\frac{h_{14}}{2c\epsilon_r}\right)^2\frac{e^2}{2q}. \tag{85}$$

This corresponds to the 3D$\rightarrow$2D transformation of the Coulomb potential, i.e., $1/|\vec{q}|^2 \rightarrow 2/q$. Finally, we get

$$r = -\frac{\pi\epsilon_0}{\rho_i\epsilon_r}\left(\frac{h_{14}}{c}\right)^2 = -1.5\times 10^{-5}. \tag{86}$$

Hence, the 2D piezoelectric contribution is also negligible.

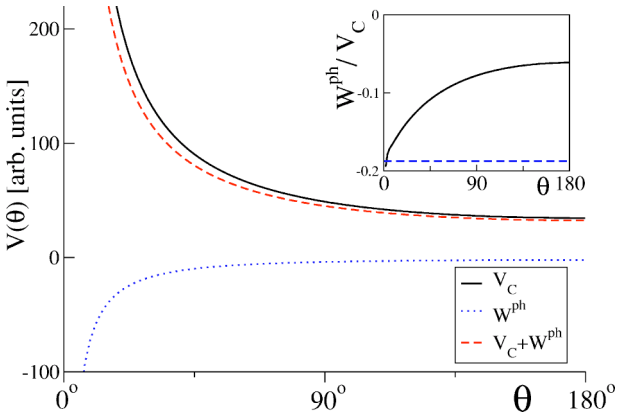

FIG. 10. Effective 2D *e-e* interaction $W_{2D}^{\rm ph}$ from LO polar phonons as a function of the scattering angle θ. We take a well with a width $d=5$ nm, and fix $q=2k_F\sin(\theta/2)$ and $\omega=0$. We compare it to the unscreened Coulomb interaction V_C. Inset: Ratio $\mathcal{R}=W_{2D}^{\rm ph}/V_C$ from (91); the horizontal line corresponds to the small-q approximation (90).

D. Optical phonons: Polar coupling

The electron-phonon matrix element is[5]

$$M(\vec{q})=\sqrt{\left[\frac{1}{\epsilon(\infty)}-\frac{1}{\epsilon(0)}\right]\frac{2\pi e_0^2}{|\vec{q}|^2}\hbar\omega_{LO}V}, \tag{87}$$

where $\epsilon(0)$ and $\epsilon(\infty)$ are the static- and high-frequency dielectric constants. For $\omega=0$, this yields

$$W^{\rm ph}(\vec{q})=-\left[\frac{1}{\epsilon(\infty)}-\frac{1}{\epsilon(0)}\right]\frac{4\pi e_0^2}{|\vec{q}|^2}. \tag{88}$$

Hence, the effective 2D potential is, for small q,

$$W_{2D}^{\rm ph}(q)\simeq-\left[\frac{1}{\epsilon(\infty)}-\frac{1}{\epsilon(0)}\right]\frac{2\pi e_0^2}{q}, \tag{89}$$

and we get the ratio

$$r\simeq-\epsilon_r\left[\frac{1}{\epsilon(\infty)}-\frac{1}{\epsilon(0)}\right]=-19\,\%\,. \tag{90}$$

As the ratio $|r|$ is rather large, it is important to consider here the more accurate expression, valid for larger q, found by performing the integration (74) with the triangular well solution (71)

$$W_{2D}^{\rm ph}(q)=-\left[\frac{1}{\epsilon(\infty)}-\frac{1}{\epsilon(0)}\right]\frac{2\pi e_0^2}{q}\frac{\kappa}{8(\kappa^2-q^2)^3}\times(-3q^5+10q^3\kappa^2-15q\kappa^4+8\kappa^5), \tag{91}$$

which is plotted in Fig. 10. We find the rather unexpected result that virtual (optical) phonons give a significant contribution—the ratio is $|r|<20\%$. However, the effect of $W_{2D}^{\rm ph}$ is monotonic and will not change qualitatively the scattering of two electrons in a GaAs 2DEG.

VI. KOHN-LUTTINGER INSTABILITY

Having found the scattering vertex in lowest order, we now consider higher-order diagrams and examine whether superconducting fluctuations could have an effect on the scattering. It has been known for a long time[12] that in 3D the second-order crossed diagram Λ_3 in the irreducible vertex (see Fig. 2) can lead to a pairing instability and a transition to superconductivity. The origin lies in the susceptibility χ^0 entering $\Lambda_{2,3}$; being nonanalytic, its spherical harmonics have a polynomial asymptotic decay $\chi_l^0\sim l^{-4}$ with respect to the coefficient l of the spherical harmonics decomposition, while the single interaction is analytic and, therefore, yields $v_l\sim e^{-l}$. As χ_l^0 oscillates, the irreducible vertex becomes attractive for sufficiently large l, $\Lambda_l\sim v_l^0+\Lambda_{3,l}<0$. The transition temperature is found from the Cooper divergence of Γ, i.e., by the relation $1=\nu_{3D}\Lambda_l$, where ν_{3D} is the same as Eq. (32) with the 2D density of state $m/2\pi\hbar^2$ replaced by the 3D one. This yield an infinitesimal temperature,[12] $k_BT_c\sim\exp(-10^5)$ for a metal with $r_s=4.5$.

In 2D the equivalent transition does not occur because there is no instability for particles below the Fermi surface; $q<2k_F$ and $\chi^0=-N_0$ have no (negative) harmonics. It has been shown, however, that higher-order diagrams (in Λ) can lead to a transition.[13] Alternatively, finite energy transfers can induce "pseudopairing" in the *d*-wave Cooper channel.[17] In our work, however, we are not interested in a superconducting transition; rather, we would like to verify that the scattering vertex for the injected particles, which are above the Fermi surface, is not substantially renormalized by the standard (lowest-order) Kohn-Luttinger instability with no energy transfer.

The singular part of $\Lambda_{2,3}$ originates from the function $B(\mathbf{k},\tilde{q})$ evaluated near $\tilde{q}=0$. Neglecting the variations of V in the q integrals [Eqs. (24) and (25)] (this corresponds to approximating $V(r)$ by a very short-range potential, e.g., a δ function), we evaluate V at the singular points of B and write

$$\Lambda_2\simeq 2V(0)V(2k_F)\int d\mathbf{k}_1B(\mathbf{k}_1,\tilde{q})=-V(0)V(2k_F)\chi^0(\tilde{q}), \tag{92}$$

$$\Lambda_3\simeq V^2(0)\int d\mathbf{k}_1B(\mathbf{k}_1,\tilde{Q})=-V^2(0)\chi^0(\tilde{Q})/2, \tag{93}$$

where $q=|\mathbf{p}'-\mathbf{p}|\simeq 2k_F$ and $Q=|\mathbf{p}'+\mathbf{p}|\simeq 2k_F$. We see that we can neglect $\Lambda_2\sim r_s\Lambda_3$; we also take the static limit (19) of $\chi^0(\omega)$ as it varies on a scale $\sim E_F$. As Q should be slightly above $2k_F$, we take

$$Q=k_F(2+c)\cos\,\theta/2 \tag{94}$$

with $c=\xi/E_F\simeq 2(p-k_F)/k_F\ll 1$ and $|\theta|\ll 1$. The Fourier coefficients of the crossed diagrams are therefore given by

$$\Lambda_{3,n}=V^2(0)\frac{1}{2\pi}\int_0^\pi d\theta\cos(n\theta)\frac{m}{\pi\hbar^2}\left[1-\Theta(\bar{\theta}-\theta)\times\left(\sqrt{1-\frac{1}{(1+c/2)^2\cos^2(\theta/2)}}\right)\right], \tag{95}$$

with $\bar{\theta}\simeq\sqrt{2c}$. In lowest order in c, we find for the singular part

$$\Lambda_{3,n} = V^2(0)\frac{m}{2\pi\hbar^2}\frac{\overline{\theta}}{4n}J_1(n\overline{\theta}) \tag{96}$$

and the asymptotics

$$\overset{n\gg 1}{\Lambda_{3,n}} \simeq V^2(0)\frac{m}{8\pi\hbar^2}\sqrt{\frac{\pi\overline{\theta}}{n^3}}\sin(n\overline{\theta}-\pi/4), \tag{97}$$

compared[12] to l^{-4} in 3D. Note the oscillatory behavior, which allows for negative values. The instability temperature can be estimated by requiring

$$|\Lambda_{3,n}| \geqslant v_n \Rightarrow n > n_0 = \frac{4}{\pi r_s^2\overline{\theta}}, \tag{98}$$

where we neglected the oscillating sine function and used Eq. (46) for v_n. We find

$$k_BT \sim E_Fe^{-1/|\Lambda_{3,n_0}|} \simeq E_Fe^{-4/r_s^3c}. \tag{99}$$

Note that the parameter c appears in 2D because of the Θ function in Eq. (19) and is absent in 3D. For GaAs and taking $c=0.02$, we find $k_BT/EF \sim e^{-100}$, which means that the attractive effect of the crossed diagram is completely negligible and does not lead to any sizable fluctuations of the scattering vertex. For a metal with $r_s \simeq 4.5$, the transition temperature in 3D was found[12] to be $\sim E_Fe^{-40\,000}$. In 2D, we cannot neglect the sine as in Eq. (98); numerically, we find the temperature $\sim E_Fe^{-20/c}$. This can be larger than in 3D for $c>10^{-4}$, despite the fact that the asymptotic decay of $v_n \sim n^{-2}$ is much slower than in 3D ($v_l \sim e^{-l}$).

VII. CONCLUSION

The prospect of experiments probing individual electron collisions in a 2DEG is a natural motivation to study the problem of two electrons interacting via Coulomb interaction in the presence of a Fermi sea. One of the main results of this work is the expression (38) for the scattering amplitude for two electrons in the Cooper channel. We found that the presence of the Fermi sea yields a significant renormalization of the strength of the scattering, rather similar to the renormalization found in the discussion of the Cooper instability. This is closely linked to the selection of intermediate states at the Fermi surface. Away from the Cooper channel, this selection disappears and the Born approximation is valid. The overall angular dependence is fairly unmodified and smooth. There is a sizable dependence on the sheet density, while the dependence on temperature, energy, and impact angle is strongly influenced by the Fermi occupation factors. The total scattering length is $\lambda_{\mathrm{tot}} \simeq 3$ nm, which is of the same order as the Fermi wavelength.

We discussed how to use such collisions to produce EPR pairs at a scattering angle of $\theta=\pi/2$. This mechanism is rather robust against imprecisions in θ, for an output singlet current around 0.5 pA. The EPR production was found to be slightly more efficient in the case of hot electrons. We discussed detection of entanglement and quantum interference and proposed a way to create localized EPR pairs separated by mesoscopic distances.

We studied phonon-mediated electron-electron interaction. We found that the dominant contribution comes from polar coupling to optical phonons, but does not affect qualitatively the Coulomb scattering. The strength of the Kohn-Luttinger superconducting instability was calculated and shown to be negligible. Finally, we developed (in Appendix B) an alternative calculation valid for diverging forward-scattering contributions and showed them to be negligible in GaAs.

ACKNOWLEDGMENTS

We thank C. Egues, V. Golovach, W. Coish, A. Bleszynski, B. Lee, and M. Yildirim for useful discussions. This work has been supported by NCCR "Nanoscale Science", Swiss NSF, EU-Spintronics, DARPA, ARO, and ONR.

APPENDIX A: SMALL r_s APPROXIMATION AT $\theta=\pi/2$

Here we derive analytical expressions for the t matrix and its derivative at $\theta=\pi/2$, which we then use to compute the ratio R. We first note that $t(\pi/2)$ is an alternating series

$$t(\pi/2) = t_0 + 2\sum_{n>1}(-1)^n t_{2n}, \tag{A1}$$

where $t_n=v_n/(1-\nu v_n)$. We write the differences as $t_n-t_{n+2} = h_n/[(1-\nu v_n)(1-\nu v_{n+2})]$ with $h_n=v_n-v_{n+2}$, which allows us to get the smoother series

$$t(\pi/2) = \frac{h_0}{(1-\nu v_0)(1-\nu v_2)} - \frac{h_2}{(1-\nu v_2)(1-\nu v_4)} + \cdots. \tag{A2}$$

Now we use for the denominators the very small r_s approximation (47) $v_n \simeq -\overline{v}\log r_s$, $\overline{v}=2e_0^2/k_F$, giving

$$t(\pi/2) = \frac{1}{(1+\nu\overline{v}\log r_s)^2}(h_0 - h_2 + h_4 - h_6 + \cdots). \tag{A3}$$

For the numerators we write

$$h_n = 2\overline{v}\left(\frac{\cos\gamma}{2n+1} + \frac{\cos 3\gamma}{2n+3}\right) + 2\overline{v}\left\{\frac{\cos 5\gamma - \cos\gamma}{2n+5} + \frac{\cos 7\gamma - \cos 3\gamma}{2n+7} + \cdots\right\} \tag{A4}$$

and neglect the second term, which is of order r_s. Then

$$t(\pi/2) = \frac{2\overline{v}}{(1+\nu\overline{v}\log r_s)^2}\sum_{n>0}(-1)^n\left(\frac{1}{4n+1} + \frac{1}{4n+3}\right), \tag{A5}$$

and, finally,

$$t(\pi/2) = \frac{2\overline{v}}{(1+\nu\overline{v}\log r_s)^2}\frac{\pi}{2\sqrt{2}}. \tag{A6}$$

This approximation is good for very low r_s; the error is $\sim 10\%$ for $r_s<0.09$, which corresponds, however, to a very high density $n=4\times 10^{17}$.

We proceed similarly for the derivative $t'(\pi/2)$

$$t'(\theta/2) = 2(-t_1 + 3t_3 - 5t_5 + 7t_7 - 9t_9 + \cdots) \quad \text{(A7)}$$

$$\simeq \frac{4\bar{v}}{(1+\nu\bar{v}\log r_s)^2} \times \sum_{n>1} (-1)^n n\left(\frac{1}{4n-1} + \frac{1}{4n+1}\right). \quad \text{(A8)}$$

The sum yields $-\pi/8\sqrt{2}+\frac{1}{4}(-1)^N$ with $N\to\infty$. Neglecting the oscillating term,[53] we get

$$t'(\pi/2) = \tfrac{1}{2}t(\pi/2). \quad \text{(A9)}$$

We find in this approximation a very simple form for the ratio

$$R(\theta,\delta\theta) = \tfrac{1}{4}\delta\theta^2. \quad \text{(A10)}$$

This corresponds to the Born approximation result [Eq. (62)] in the limit of no screening ($r_s\to 0$). This is somewhat surprising, as our result (A6) still contains both the screening (finite r_s) and the resumed higher-order terms (responsible for the term $\nu\bar{v}$ in the numerator). One must further expand $t(\pi/2)$ in small r_s in order to recover the Born approximation with an unscreened potential

$$t(\pi/2) \simeq \bar{v}\frac{\pi}{\sqrt{2}} = r_s\pi\frac{\hbar^2}{m} = V_C(q = k_F\sqrt{2}). \quad \text{(A11)}$$

The Fourier series is not well defined in this case because of the forward-scattering divergence $V_C(0)$. We also note that the number of Fourier coefficients required to reach convergence of the numerical Fourier sum increases dramatically to $n_{max}=70\,000$ for $n=10^{23}$ (with the heuristic dependence $n_{max}\sim r_s^{-0.8}$), as the potential becomes more peaked.

APPENDIX B: FORWARD SCATTERING WHEN $r_s\to 0$

Here we consider carefully the limit of vanishing $r_s\to 0$, by following a different approach to solve the Bethe-Salpeter equation, which allows us to study the contribution of forward-scattering states. These are indeed important in the very small r_s limit, as the *unscreened* Coulomb-scattering cross section has a forward-scattering divergence (i.e., for vanishing momentum transfers, $q=0$) in 3D and 2D.

The calculation that was presented in Sec. III is based on the logarithmically dominant contribution of $\nu\sim\log c$ with $c=\max(k_BT,\xi)/E_F$; it is a many-body effect related to the sharp edge of the Fermi surface that occurs only in the Cooper channel $\mathbf{p}_2=-\mathbf{p}_1$. This approach fails in the situation where r_s is very small, when the screening is too small to reduce the forward divergence of the unscreened Coulomb potential. In this situation, one must carefully consider the contribution of forward-scattering intermediate states with $q=|\mathbf{k}-\mathbf{p}|\simeq 0$ as they yield at large term $V\sim 2\pi e_0^2/k_s$. For such states, one must keep the restriction $k\simeq p\simeq k_F$, but consider the contribution of small angles $\phi=\angle(\mathbf{k},\mathbf{p})$, defined by[54]

$$\phi, |\phi-\theta| \ll \bar{\phi} = \frac{d}{p} \to \frac{\delta}{p} = \frac{p-k_F}{p} \simeq \frac{c}{2} \ll 1, \quad \text{(B1)}$$

where $d=k-k_F$, $\delta=p-k_F$, and $\theta=\angle(\mathbf{p},\mathbf{p}')$ is the scattering angle. This corresponds to the forward scattering into *virtual* states; we do not yet specify the real scattering angle θ between the initial and final states. We now go back to the iterations of the Bethe-Salpeter, after the frequency integration (30), still considering only the Cooper channel.

1. Angular integral

We introduce the polar notation $\mathbf{k}_i=(k_i,\phi_i)$ and write the potential $V(k_1,\phi_1;k_2,\phi_2)\equiv V(\mathbf{k}_1-\mathbf{k}_2)$, assuming $\mathbf{p}=(p,0)$, $\mathbf{p}'=(p,\theta)$. We first consider the angular integrals for the nth order iteration of the Bethe-Salpeter equation

$$\frac{1}{2\pi}\int_{-\bar{\phi}}^{\bar{\phi}} d\phi_1 V(p,\theta;k_1,\phi_1)\frac{1}{2\pi}\int_{-\bar{\phi}}^{\bar{\phi}} d\phi_2 V(k_1,\phi_1;k_2,\phi_2)\times\cdots\times\frac{1}{2\pi}\int_{-\bar{\phi}}^{\bar{\phi}} d\phi_{n-1} V(k_{n-2},\phi_{n-2};k_{n-1},\phi_{n-1})V(k_{n-1},\phi_{n-1};p,0)$$
$$\simeq \left(\frac{\bar{\phi}}{\pi}\right)^{n-1} \underbrace{V(p,\theta;k_1,0)V(k_1,0;k_2,0)\ldots}_{=a_\theta a^{n-3}} \underbrace{V(k_{n-2},0;k_{n-1},0)V(k_{n-1},0;p,0)}_{=b(k_{n-2},k_{n-1})}. \quad \text{(B2)}$$

2. Energy integral

First we consider

$$b(k',k) = \frac{2\pi e_0^2}{k_s+|k'-k|}\frac{2\pi e_0^2}{k_s+|k-p|}. \quad \text{(B3)}$$

We truncate the energy integration to a small range $k\in[k_F=p-\delta,p+\delta]$ around p and define $B(k')\coloneqq(1/2\pi)\int_{k_F}^{k_F+2\delta}dk k D(k)b(k',k)$. We can expand the lengthy result in the lowest order in k_s and find

$$B(k') \simeq i\frac{m\pi^2 e_0^4}{\hbar^2 k_s|k'-p|}[1+\mathcal{O}(k_s/p)]. \quad \text{(B4)}$$

Thus, the subsequent k' integration will be mainly given by a small region around $k'=p$, as expected. Hence one should set

$k'=p$ in the exact result $B(k')$ before expanding in lowest order of k_s, which yields

$$B(k'=p) \simeq i\frac{m\pi^2 e_0^4}{\hbar^2 k_s^2}[1+\mathcal{O}(k_s/p)]. \tag{B5}$$

For the integration of $a(k)$ in $A:=(1/2\pi)\int_{k_F}^{k_F+2\delta} dkkD(k)a(k)$, we set $k'=p$ and expand the result. This gives

$$A \simeq -i\frac{m\pi e_0^2}{2\hbar^2 k_s}[1+\mathcal{O}(k_s/p)]. \tag{B6}$$

For the last term containing the scattering angle $A_\theta := (1/2\pi)\int_{k_F}^{k_F+2\delta} dkkD(k)a_\theta(k)$, we have

$$A_\theta \simeq = -i\frac{m\pi e_0^2}{2q\hbar^2}[1+\mathcal{O}(k_s/p)] = A\frac{k_s}{q} \tag{B7}$$

with $q=2k_F \sin|\theta/2|$. Writing the series $t=\Sigma_n t^{(n)}$, we find for the nth-order term $(n>0)$

$$t^{(n)} = \left(\frac{\phi}{\pi}\right)^{n-1} A^{n-1}A_\theta B = \frac{2\pi e_0^2}{q}D^{n-1}, \tag{B8}$$

with

$$D = \frac{i}{8\pi}c = \frac{i}{8\pi}\frac{\xi}{E_F}. \tag{B9}$$

3. Result

So far we have only considered the case where all intermediate angles are $\phi_i=0$, $i=1,\ldots n$, and only the final angle is the scattering angle θ. There are n equivalent cases giving the same contribution, where the first j angles are zero and the remaining ones are $\phi_i=\theta, j<i\leqslant n$. Thus the expansion series of the Bethe-Salpeter Equation is $t=V+\Sigma_{n>0} nt^{(n)}$. Performing the summation, we get the scattering t matrix for Coulomb scattering in the limit of very small $r_s \ll 1$

$$t = \frac{2\pi e_0^2}{q+k_s} + \frac{2\pi e_0^2}{q}D\frac{2-D}{(1-D)^2} \overset{k_s \ll q}{=} \frac{2\pi e_0^2}{q}\frac{1}{(1-D)^2}, \tag{B10}$$

with $q=2k_F \sin|\theta/2|$. We can further expand this result in $D\ll 1 \Rightarrow t \simeq 2\pi e_0^2/q = V_C$; however, this merely reflects the fact that the Born approximation with unscreened potential is accurate in the limit $r_s \to 0$ because e_0^2 is also proportional to r_s. We also note that with this result the scattering amplitude has a phase $2\arctan|D| = 2\arctan(\overline{\phi}/8\pi)$. However, it is independent from the angle θ and, therefore, does not yield quantum oscillations in the singlet and triplet scattering lengths as discussed in Sec. IV F.

In the case of forward scattering[55] with $\theta=0$, the counting of equivalent arrangements of the intermediate states gives a factor of 2^n instead of n. The result has a more familiar form,

$$t = \frac{2\pi e_0^2}{k_s}\frac{1}{1-2D}. \tag{B11}$$

As expected, the forward-scattering amplitude (B11) is larger than (B10) by a factor of $\sim q/k_s \sim 1/r_s$.

4. Comparison

We now compare the nth-order obtained here, $t_{r_s}^{(n)}$ defined in Eq. (B8) with the calculation of Sec. III, i.e., the mth Fourier coefficient $t_m^{(n)} = v_m(\nu v_m)^{n-1}$. Their ratio is

$$\frac{t_m^{(n)}}{t_{r_s}^{(n)}} = \frac{v_m q}{n2\pi e_0^2}\left(\frac{\nu v_m}{D}\right)^{n-1} \sim \frac{1}{n}\left[\log\left(\frac{k_s}{k_F}\right)\right]^n \left[\frac{k_s}{k_F}\frac{\log c}{c}\right]^{n-1}, \tag{B12}$$

where have considered the small r_s approximation (47) $v_m \simeq (2\pi e_0^2/k_F)\log(k_s/k_F)$. Therefore, the calculation of Sec. III is valid provided that

$$r_s|\log r_s| \gg \frac{\pi}{\sqrt{2}}\frac{c}{|\log c|}. \tag{B13}$$

Taking $c=\delta/k_F=0.01$, we find that we need $r_s>0.01$, which is always the case for typical semiconductor material. In conclusion, the large value of r_s does not allow one to see the contribution of forward scattering into (virtual or real) states.

[1] M. A. Topinka, B. J. LeRoy, S. E. J. Shaw, E. J. Heller, R. M. Westervelt, K. D. Maranowski, and A. C. Gossard, Science **289**, 2323 (2000); M. A. Topinka, B. J. LeRoy, R. M. Westervelt, S. E. J. Shaw, R. Fleischmann, E. J. Heller, K. D. Maranowski, and A. C. Gossard, Nature (London) **410**, 183 (2001).

[2] B. J. Leroy, J. Phys.: Condens. Matter **15**, R1835 (2003).

[3] D. S. Saraga, B. L. Altshuler, D. Loss, and R. M. Westervelt, Phys. Rev. Lett. **92**, 246803 (2004).

[4] A. L. Fetter and J. D. Walecka, *Quantum Theory of Many-Particle Systems* (McGraw-Hill, New York, 1971).

[5] G. D. Mahan, *Many-Particle Physics* (Plenum, New York, 2000).

[6] F. Stern, Phys. Rev. Lett. **18**, 546 (1967).

[7] G. F Giuliani and J. J. Quinn, Phys. Rev. B **26**, 4421 (1982).

[8] L. Zheng and S. Das Sarma, Phys. Rev. B **53**, 9964 (1996).

[9] G. Burkard, D. Loss, and E. V. Sukhorukov, Phys. Rev. B **61**, R16 303 (2000).

[10] V. M. Galitski and S. Das Sarma, Phys. Rev. B **70**, 035111 (2004).

[11] C. S. Ting, T. K. Lee, and J. J. Quinn, Phys. Rev. Lett. **34**, 870 (1975).

[12] W. Kohn and J. M. Luttinger, Phys. Rev. Lett. **15**, 524 (1965); J. M. Luttinger, Phys. Rev. **150**, 202 (1966).

[13] A. V. Chubukov, Phys. Rev. B **48**, 1097 (1993).

[14] T. Suwa, K. Takayanagi, and E. Lipparini, Phys. Rev. B **69**, 115105 (2004). In contrast to our work, these authors consider a finite total momentum $P=k_F\sqrt{2}\neq 0$ (for particles within the

Fermi sea), a 3D-like screening $V(r) \sim e^{-\mu r}/r$, large values of $r_s \sim 1-20$, and use a Bethe-Goldstone equation (which does not include the exchange process shown in our Fig. 3).

[15] M. C. Bønsager, K. Flensberg, B. Y.-K. Hu, and A. H. MacDonald, Phys. Rev. B **57**, 7085 (1998).

[16] R. Jalabert and S. Das Sarma, Phys. Rev. B **40**, 9723 (1989).

[17] V. M. Galitski and S. Das Sarma, Phys. Rev. B **67**, 144520 (2003).

[18] D. Loss and D. P. DiVincenzo, Phys. Rev. A **57**, 120 (1998).

[19] G. Burkard and D. Loss, in *Semiconductor Spintronics and Quantum Computation* (Springer-Verlag, New York, 2002).

[20] L. M. K. Vandersypen, R. Hanson, L. H. Willems van Beveren, J. M. Elzerman, J. S. Greidanus, S. De Franceschi, and L. P. Kouwenhoven, in *Quantum Computing and Quantum Bits in Mesoscopic Systems* (Kluwer Academic/Plenum, New York, 2003).

[21] P. Recher, E. V. Sukhorukov, and D. Loss, Phys. Rev. B **63**, 165314 (2001).

[22] W. D. Oliver, F. Yamaguchi, and Y. Yamamoto, Phys. Rev. Lett. **88**, 037901 (2002).

[23] D. S. Saraga and D. Loss, Phys. Rev. Lett. **90**, 166803 (2003).

[24] P. Recher and D. Loss, Phys. Rev. B **65**, 165327 (2002); C. Bena, S. Vishveshwara, L. Balents, and M. P. A. Fisher, Phys. Rev. Lett. **89**, 037901 (2002).

[25] G. B. Lesovik, T. Martin, and G. Blatter, Eur. Phys. J. B **24**, 287 (2001); G. Falci, D. Feinberg, and F. W. J. Hekking, Europhys. Lett. **54**, 255 (2001).

[26] P. Recher and D. Loss, Phys. Rev. Lett. **91**, 267003 (2003).

[27] A. T. Costa, Jr. and S. Bose, Phys. Rev. Lett. **87**, 277901 (2001); S. Bose and D. Home, *ibid.* **88**, 050401 (2002).

[28] P. Samuelsson, E. V. Sukhorukov, and M. Büttiker, Phys. Rev. Lett. **91**, 157002 (2003).

[29] C. W. J. Beenakker, C. Emary, M. Kindermann, and J. L. van Velsen, Phys. Rev. Lett. **91**, 147901 (2003).

[30] P. Samuelsson, E. V. Sukhorukov, and M. Büttiker, Phys. Rev. Lett. **92**, 026805 (2004).

[31] J. R. Taylor, *Scattering Theory* (Wiley, New York, 1972).

[32] J. Jacoby, Phys. Scr. **64**, 220 (2001).

[33] From this perspective, the experimental demonstration of the scattering of quasiparticle states would also shed light on the applicability of Fermi liquid theory in 2D; see P. W. Anderson, cond-mat/0101417 (unpublished); Phys. Rev. Lett. **71**, 1220 (1993) and Ref. [1] therein.

[34] For simplicity we call the wave vectors $(\mathbf{p}, \mathbf{k}, \mathbf{q}, \ldots)$ "momenta," and set $\hbar = 1$ for the frequencies ω.

[35] G. Barton, Am. J. Phys. **51**, 420 (1983); S. K. Adhikari, *ibid.* **54**, 362 (1986).

[36] It is only the motion of the electron that is confined in 2D; the field lines are 3D.

[37] T. Ando, A. B. Fowler, and F. Stern, Rev. Mod. Phys. **54**, 437 (1982); C. W. J. Beenakker and H. van Houten, Solid State Phys. **44**, 1 (1991).

[38] One can easily consider Z and m^* by rescaling the quantity ν defined in Eq. (30) via $\nu \to \nu \times Z^2\, m^*/m$.

[39] A. V. Chubukov and M. Yu Kagan, J. Phys.: Condens. Matter **1**, 3135 (1989).

[40] More formally, one must consider a linear expansion of the denominator of V to make the integral convergent for large k, as the decay of $D(k)$ is too slow. Alternatively, one can insert a cutoff for the integral at, e.g., $2k_F$.

[41] See e.g. *Quantum Noise in Mesoscopic Physics*, edited by Yu. V. Nazarov, NATO ASI Series II Vol. 97 (Kluwer, Dordrecht, 2003).

[42] G. B. Lesovik and L. S. Levitov, Phys. Rev. Lett. **72**, 538 (1994).

[43] G. Burkard, D. Loss, and E. V. Sukhorukov, Phys. Rev. B **61**, R16 303 (2000); J. C. Egues, G. Burkard, and D. Loss, Phys. Rev. Lett. **89**, 176401 (2002); G. Burkard and D. Loss, *ibid.* **91**, 087903 (2003); L. Faoro, F. Taddei, and R. Fazio, Phys. Rev. B **69**, 125326 (2004); P. Samuelsson, E. V. Sukhorukov, and M. Büttiker, *ibid.* **70**, 115330 (2004).

[44] S. Kawabata, J. Phys. Soc. Jpn. **70**, 1201 (2001).

[45] P. Recher, D. S. Saraga, and D. Loss, in *Fundamental Problems of Mesoscopic Physics: Interactions and Decoherence*, NATO Science Series II Vol. 154 (Kluwer, Dordrecht, 2004).

[46] P. Recher, E. V. Sukhorukov, and D. Loss, Phys. Rev. Lett. **85**, 1962 (2000); R. Hanson, L. M. K. Vandersypen, L. H. Willems van Beveren, J. M. Elzerman, I. T. Vink, and L. P. Kouwenhoven, Phys. Rev. B **70**, 241304 (2004).

[47] R. M. Potok, J. A. Folk, C. M. Marcus, and V. Umanski, Phys. Rev. Lett. **89**, 266602 (2002).

[48] R. Fiederling, M. Keim, G. Reuscher, W. Ossau, G. Schmidt, A. Waag, and L. P. Molenkamp, Nature (London) **402**, 787 (1999); Y. Ohno, D. K. Young, B. Beschoten, F. Matsukura, H. Ohno, and D. D. Awschalom, *ibid.* **402**, 790 (1999).

[49] A. North, J. Burroughes, T. Burke, A. Shields, C. E. Norman, and M. Pepper, IEEE J. Quantum Electron. **35**, 352 (1999).

[50] S. Tarucha, D. G. Austing, Y. Tokura, W. G. van der Wiel, and L. P. Kouwenhoven, Phys. Rev. Lett. **84**, 2485 (2000).

[51] V. F. Gantmakher and Y. B. Levinson, *Carrier Scattering in Metals and Semiconductors* (North-Holland, Amsterdam, 1987); see also http://www.ioffe.rssi.ru/SVA/NSM/Semicond/GaAs/basic.html

[52] P. J. Price, Ann. Phys. (N.Y.) **133**, 217 (1981).

[53] This is similar to neglecting the oscillating term in the Poisson sum $\delta(\theta = \pi) = \Sigma_n (-1)^n = 0$.

[54] The calculation in Sec. III involved the expansion $|\mathbf{k}-\mathbf{p}| = \sqrt{p^2+k^2-2pk\cos\phi} \simeq 2p\sin(\phi/2)\mathbf{(}1 + d/p + O\{d^2/[2p\sin(\phi/2)]^2\}\mathbf{)}$, which breaks down for small angles ϕ.

[55] We note that the present calculation is not strictly valid in the case of forward scattering, because of the remaining terms $O\{d^2/[2p\sin(\phi/2)]^2\}$ in (B2) which only give a negligible contribution in the integration when $\overline{\phi} \ll 2\tan\theta/2 \simeq \theta$ (preventing the limit $\theta \to 0$).